Computers and Geotechnics 177 (2025) 106902

Contents lists available at ScienceDirect

Computers and Geotechnics

journal homepage: www.elsevier.com/locate/compgeo

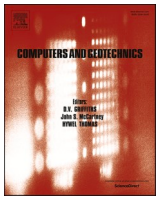

Coupled CFD-DEM modelling of clogging of granular columns by cohesive fines

Thao Doan [a], Buddhima Indraratna [a,b,*], Thanh T. Nguyen [a,b], Cholachat Rujikiatkamjorn [a,b]

[a] Transport Research Centre, Faculty of Engineering and Information Technology, University of Technology Sydney, NSW 2007, Australia
[b] Faculty of Engineering and Information Technology, University of Technology Sydney, NSW 2007, Australia

ARTICLE INFO

Keywords:
Interparticle cohesion
Clogging behaviour
Discrete element method
Computational fluid dynamic
Agglomeration behaviour

ABSTRACT

The ubiquitous phenomenon of particle migration and clogging in porous media, particularly when involving cohesive fines necessitates a critical need for in-depth understanding from a microscale perspective. Therefore, this study aims to elucidate the migration and clogging behaviour of polydisperse cohesive fines across a granular medium by using the coupled Computational Fluid Dynamics-Discrete Element Method (CFD-DEM). Primary governing factors including the relative coarse–fine size ratio and the strength of interparticle cohesive force through the concept of bond number are examined in detail from both macro- and micromechanical perspectives. The results reveal that the presence of interparticle cohesion drastically modifies the migration of fine particles, associating with a notable reduction in the infiltration ratio and an increased likelihood of particle deposition. This study innovatively explores the combined effect of the coarse–fine size ratios and cohesive strength on the migratory behaviour of fines through the infiltration ratio and critical time ratio, whereby clogging carries substantial implications on the geo-hydraulic performance of the granular medium. Moreover, in the context of cohesive fines, the Authors propose a comprehensive and novel algorithm for detecting and analysing cohesion-induced agglomeration effect. The results reveal that the formation and breakage of agglomerates due to the metastability of cohesive bonds between fines can be captured to explain the unstable flows occurring through the clogged zones.

1. Introduction

The migration of suspended fine particles across porous media under fluid flow is ubiquitous in various natural and engineering processes, ranging from sediment transport to applications of filtration and drainage systems in geotechnical engineering. For instance, the fluid flowing through a granular assembly such as permeable reactive barriers and gravel columns can transport fine particles such as silts and clays, of which a certain fraction can be retained within the pore structure causing clogging. This phenomenon can significantly alter porous features and corresponding hydraulic properties of the granular medium, seriously affecting the infiltration and discharge capacity of the system. For example, Pal and Deb (2019) shows that clogging can substantially reduce permeability of stone columns, resulting in more than 50 % increase in excess pore pressure. Another example of clogging is the upward migration of fluidised subgrade soil into the overlying sub-ballast and ballast layers causing mud pumping and ballast fouling. Various site investigations into mud pumping railways have proved that the contamination of ballast by infiltrated fines does not only reduce the drainage capacity of the foundation, but also deteriorates the frictional contacts between coarse particles, thus decreasing shear strength (Nguyen and Indraratna, 2022; Tennakoon et al., 2014). Similarly, in drainage filters of varying systems such as prefabricated vertical drains (PVDs) (Nguyen and Indraratna, 2019; Xu et al., 2022), sand filters (Reddi and Bonala, 1997), and granular media such as stone columns (Indraratna et al., 2013), the clogging effect remains a prevalent and critical challenge. Therefore, understanding and mitigating the clogging phenomenon is essential to ensure the long-term effectiveness and stability of granular media used across various geotechnical infrastructure.

Numerous experimental studies have been conducted to examine the susceptibility of fine migration and its subsequent potential for particle deposition/clogging, focusing on three main governing aspects such as geometric factors (i.e., fabric, particle size distribution, and constriction size distribution, etc.) (Tang et al., 2020); hydraulic conditions (i.e., hydraulic gradient and flowing velocity) (Rao et al., 2022); and stress states (i.e., confining pressures and anisotropic stress ratio) (Chen et al.,

* Corresponding author.
E-mail address: buddhima.indraratna@uts.edu.au (B. Indraratna).

https://doi.org/10.1016/j.compgeo.2024.106902
Received 29 May 2024; Received in revised form 17 October 2024; Accepted 5 November 2024
Available online 12 November 2024

2017). Moreover, mathematical models (Locke et al., 2001; Reddi and Bonala, 1997) have been developed to predict particle migration and internal erosion through variations in particle and constriction size distributions and mass conservation. While many macroscale phenomena such as changes in hydraulic conductivity and particle size distribution can be observed and determined in experimental and analytical studies, the detailed micromechanics underpinning the hydro-mechanical response of the granular assembly remains unclear. For instance, when migration occurs, the multiphase (solid–fluid) and time-dependent interactions between the coarse and fine materials under the influence of fluid flow cannot be directly obtained using conventional experimental methods (often infeasible due to the complexity of testing apparatus and instrumentations). On the other hand, traditional analytical/mathematical methods based on continuum mechanics cannot usually capture details at particle- and pore-scale, resulting in missing information and incomplete understanding. For instance, a significant problem of past studies (Basack et al., 2018; Tai et al., 2017) was the lack of an efficient methodology to quantify the time-dependent rate and extent of the clogging process, partly attributed to the complexity in monitoring these internal variations. In fact, understanding this matter is the key for estimating the critical time at which the hydraulic behaviour of granular columns is notably impacted by the clogging phenomenon.

In recent years, combinations of solid–fluid modelling techniques commonly known as computational fluid dynamics (CFD) coupled with discrete element method (DEM) have been increasingly used to capture multiphase systems in particulate detail (Nguyen and Indraratna, 2020; Tao and Tao, 2017; Zhao and Shan, 2013). The topic of computational fluid dynamics (CFD) generally consists of two main branches: unresolved and resolved techniques (Anderson and Wendt, 1995; Tsuji et al., 1992). The unresolved CFD approach, simply referred to as CFD, employs averaged fluid parameters such as the fluid pressure, velocity and porosity in fluid cells to solve the governing equations (normally based on Navier-Stokes theories). In contrast, the resolved technique such as Lattice Boltzmann Method (LBM) can simulate fluid at very fine scale by discretising the fluid into a large number of fictive particles and facilitating more intricate fluid–solid interactions, e.g. detailed migration of fines around coarse particles (Indraratna et al., 2021; Parvan et al., 2020; Zhou et al., 2020). However, LBM often requires much finer spatial and temporal resolutions, leading to a limited number of particles and excessive computational effort. Therefore, the unresolved CFD-DEM method has been more commonly adopted to understand the mechanisms which govern fines migration and clogging processes (Tao and Tao, 2017; Xiong et al., 2022). For example, Zhang et al. (2023) performed filtration simulations on mono-disperse fine and coarse samples and distinctly observed the transitions of filtration process from "no infiltration" to "continuing infiltration" with increasing size ratios from 5 to 10. Liu et al. (2020) observed that gap-graded soils with higher fines content exhibited a higher susceptibility to clogging and clogged fines tended to decrease the localised permeability and lead to the development of preferential flow paths. Xiong et al. (2022) discovered the dynamic nature of clogging in cohesionless fines, which is highly dependent on various factors including the size of coarse materials, the velocity of the flow, and the amount of fines present. Table 1 assembles some of the most recent numerical studies focused on the clogging caused by the entrapment of fine particles within various coarse media, followed by a discussion on limitations in terms of the simulated loading conditions, and the type of interactions between fine and coarse particles. For instance, although these studies have provided valuable insights into the migration and clogging behaviour of fines with various influencing factors (Table 1), they have often ignored the interparticle cohesion existing between fine particles. When cohesion is considered, attractive forces between particles can significantly change the contact behaviour amongst fines and between fine and coarse particles under fluid flow. Moreover, the complex procedure of forming and breaking agglomerates of migrating fines under varying levels of cohesion and

Table 1
Numerical clogging studies (CFD-DEM coupling) reported in the literature.

Studies	Coarse materials D_g (mm)	Fine materials D_f (mm)	Influencing factors	Research gaps in past studies
(Xiong et al., 2022)	3.3 – 7.2	0.5–1.3	• Various PSD of coarse • Inflow fine concentration	• No cohesive effect between fines is considered. • Time-dependent migration and clogging process to determine practical design parameters is not discussed.
(Elrahmani et al., 2023)	0.2 – 0.4	0.005–0.015	• Pore space geometry with initial porosities • Fine sizes	• The agglomeration effect induced by interparticle cohesion is not discussed • Consider coarse particles as rigid wall elements, they do not change their position during interaction and flow, thus no dilatancy and deformation.
(Xie et al., 2023)	0.5	0.0335–0.075	• Different size ratios between coarse and fines. • Inflow fine concentration	• Clustering behaviour of cohesive fines is not quantified in the context of soil clogging. • Vertical migration of fines is considered that is not relevant to soil-granular columns.
(Zhou et al., 2021)	0.0185–0.1	0.004	• Inflow fine concentration • Fluid flow velocity	• No quantitative data was given to quantify the agglomeration effect. • No external loading was applied to stimulate vertical and confining pressures.
(Zhang et al., 2023)	5–10	1	• Various coarse sizes • Fluid flow velocity	• No loading is applied to simulate the confining pressure. • Detailed contact interactions between coarse and fine are not discussed.
(Lin et al., 2022; Yin et al., 2021)	0.428 – 1	0.06–0.14	• Various size ratio • Fluid flow velocity • Varying cohesion levels	• The monodispersed size is not representative of real soil with varying sizes and pore structures. • Detailed contact interactions between coarse and fine are not discussed.
(Shi et al., 2021; Shi et al., 2018)	Prefabricated vertical drains (0.1 mm)	0.001	• Different fine sizes • Varying pore pressure gradient	• PVD was simulated as a fixed element in space without deformation during infiltration and clogging process. PVD has totally different porous and filter features compared to granular columns. • Cohesive force is ignored in this study.

fluid flow rates has not been quantified in any past studies (Table 1). Moreover, to the best of the authors' knowledge, none of the numerical studies (as shown in Table 1) have investigated the interplay between the coarse–fine size ratios and cohesive strength on the migratory and clogging behaviour of fines. The above limitations and insufficient understanding has posed a significant demand for investigating on the microscale evolution of soil migration and clogging considering the role of interparticle cohesion through fluid-particle coupling.

This study, therefore, aims to address the above gaps by employing the CFD-DEM framework to investigate the migration and clogging behaviour of cohesive fines across a granular medium under horizontal fluid flow. Critical influencing factors are investigated in detail, including the geometric size ratio between the coarse and fine materials, the varying degrees of cohesion of fines, and the combined effect of these factors. The coarse–fine size ratios were selected from 5.5 to 10 to encompass a wide range of filtration responses as observed in the previous study (Zhang et al., 2023). This study offers valuable insights through both macroscale results including infiltration ratios, localised distribution of fines, and deposition coefficient and microscale analysis such as contact behaviour between coarse and fine particles, and contact force evolution. More importantly, individual movements of fine particles can be obtained to monitor the temporal and spatial distributions of cohesive fines deposited within the porous medium, allowing the varying size of clogged and unclogged zones to be determined over time. These numerical results enable crucial design parameters such as the critical time and reduced permeability to be rationalised in a way that is beneficial to practical situations. Finally, the innovation of this research lies in the current attempt to quantify a cohesion-induced agglomeration process, highlighting its significance in governing the migration and clogging behaviour of cohesive fines within a granular medium.

2. Theoretical background: Governing equations

2.1. Discrete element method

At the particle scale, translational and rotational motions of particles can be captured by the Newton' second law of motions as follows:

$$m_i \frac{d\boldsymbol{U}_{pi}}{dt} = \sum \left(\boldsymbol{F}_c^{ij} + \boldsymbol{F}_{coh}^{ij}\right) + \boldsymbol{F}_g^i + \boldsymbol{F}_f^i \tag{1}$$

$$I_i \frac{d\boldsymbol{\omega}_{pi}}{dt} = \sum \left(\boldsymbol{M}_c^{ij} + \boldsymbol{M}_r^{ij}\right) + \boldsymbol{M}_f^i \tag{2}$$

where $\boldsymbol{U}_{pi}$ and $\boldsymbol{\omega}_{pi}$ denote the translational and angular velocities of the particle i respectively while m_i and I_i represent its mass and inertia moment. $\boldsymbol{F}_c^{ij}$ and $\boldsymbol{M}_c^{ij}$ correspond to the contact forces and torques in the normal and tangential directions imposing on particle i by particle j; $\boldsymbol{F}_{coh}^{ij}$ represents the additional cohesive force between two particles i and j while $\boldsymbol{F}_i^g$ is the self-weight of particle i;$\boldsymbol{F}_f^i$ and $\boldsymbol{M}_f^i$ are the force and torque induced by fluid on particle i; $\boldsymbol{M}_r^{ij}$ is the torque resisting the rotational movement between two particles..

In DEM simulations, the Hertzian theory which has been commonly used to represent the contact behaviour of particulate materials (Zhu et al., 2007), is employed in this study. Particularly, the normal $\boldsymbol{F}_{cn}$ and tangential $\boldsymbol{F}_{ct}$ contact forces are computed with respect to their corresponding stiffnesses k_n and k_t at the contact as follows:

$$k_n = \frac{4}{3} E^* \sqrt{R^* \delta_n} \tag{3}$$

$$k_t = 8G^* \sqrt{R^* \delta_n} \tag{4}$$

where R^*, E^* and G^* account for the equivalent radius, Young's and shear moduli of two contacting particles; δ_n is the relative normal overlap. Detailed procedures to determine these parameters are provided elsewhere (Zhu et al., 2007).

Amongst cohesive fines, there exists a number of attractive interactions such as van der Waals, electrostatic, and capillary forces at the periphery of particle contacts (Zhu et al., 2007). Among them, capillary force changes significantly with water content and becomes vanished approaching the saturated state, but electrostatic forces such as clay particles can exist in various contexts such as fines clogging. The complexity of these micro-scale forces, which can manifest either individually or simultaneously, makes their modelling highly variable and computationally intensive. To overcome these challenges, physic-based cohesive models such as the Johnson, Kendall and Roberts (JKR) model (Johnson et al., 1971) and the Derjaguin, Muller and Toporov (DMT) model (Derjaguin et al., 1975) have been developed to encapsulate the attractive forces at particle contacts, incorporating various particle deformation modes. Previous investigations showed that the JKR model can yield results that align closely with experimentally measured microscale cohesive forces (Barthel, 2008; Jones, 2003), therefore, this model is often referred. Moreover, the JKR model and its simplified version, the SJKR model, have been successfully applied in numerous studies to simulate a wide range of cohesive forces in the presence of fluids. For example, Tsunazawa et al. (2016) demonstrated the model's ability to accurately capture liquid-bridging forces, producing computational results that aligned well with experimental observations. Similarly, Yin et al. (2021) extended the application of the JKR model to simulate cohesive forces in fluid-saturated environments, further showcasing its versatility. The JKR model quantifies cohesive forces ($\boldsymbol{F}_{coh}^{ij}$) based on the interfacial surface energy between two particles (γ_E) and the contact radius (a) as presented in Parteli et al. (2014), as follows:

$$\boldsymbol{F}_{coh}^{ij} = 4\sqrt{\frac{\pi a^3 \gamma_E E^*}{2(1-\nu^2)}} \tag{5}$$

Although the JKR model is theoretically sound, JKR contact radius needs to be quadratically computed and therefore leads to excessive computation cost. To make the numerical model more feasible for real-life systems containing a large number of particles, a simplified JKR model (SJKR) can be considered. Previous studies (Ajmal et al., 2020; Grima, 2011) showed that this simplified cohesive model was sufficient to demonstrate the influence of microscale cohesion, thus eliminating the need for an explicit and time-intensive modelling process of non-contact cohesive forces. In the SJKR model, a numerical term called Cohesion Energy Density (CED) is used alternatively with the surface energy parameter, which is defined as the amount of energy per unit volume required to overcome the attractive interactions and detach two adjacent particles (Ucgul et al., 2014). Moreover, the SJKR model assumes that the contact deformation is elastic and the area of contact follows a circular pattern (Coetzee, 2020). This model determines the cohesive force directly from the cohesive parameter (CED) and the circular contact area (A) as follows (Doan et al., 2023):

$$\boldsymbol{F}_{coh}^{ij} = CED \bullet A \tag{6}$$

2.2. Computational fluid dynamics

Computational Fluid Dynamics (CFD) is employed to numerically solve the continuity equations (i.e., mass and momentum conservation) based on the modified Navier-Stokes (NS) theories accounting for granular particles in the fluid as follows:

$$\frac{\partial n_f}{\partial t} + \nabla \bullet \left(n_f \boldsymbol{U}_f\right) = 0 \tag{7}$$

$$\frac{\partial (n_f \rho_f \boldsymbol{U}_f)}{\partial t} + \nabla \bullet \left(n_f \rho_f \boldsymbol{U}_f \boldsymbol{U}_f\right) = -n_f \nabla p \boldsymbol{I} + \nabla \bullet \left(n_f \boldsymbol{\tau}_f\right) + n_f \rho_f \boldsymbol{g} - \boldsymbol{f}_p \tag{8}$$

where n_f, $\boldsymbol{U}_f$ and p are the averaged porosity, velocity and pressure in a computed fluid domain; ρ_f and $\boldsymbol{\tau}_f$ are the density and the viscous stress

of fluid; $\boldsymbol{I}$ is the identity vector and $\boldsymbol{g}$ is the gravitational tensor; $\boldsymbol{f_p}$ is the average fluid-particle interaction force concerning the presence of solid particles in the fluid phase. The subscriptions f and p denote fluid and particle, respectively.

The current study employs a finite volume method (FVM) to solve the modified NS equations by discretising the domain of interest into a finite number of meshes and then solving the governing equations using the locally averaged velocity and pressure of each controlled volume. The average fluid-particle force $\boldsymbol{f_p}$ in a CFD cell is computed by:

$$\boldsymbol{f_p} = \sum_{i=1}^{n_p} \overline{\omega}_i \left(\frac{\boldsymbol{F_f^i}}{V_c} \right) \tag{9}$$

where n_p is the total particle number in a cell having a volume of V_c; $\boldsymbol{F_f^i}$ is the total fluid force imposing on particle i. It is worth noting that as a fluid cell might not contain all particles fully, the contribution of each individual particle to the fluid-particle force $\boldsymbol{f_p}$ within a cell is proportionated by a factor $\overline{\omega}_i$. The factor $\overline{\omega}_i$ denotes a ratio between the occupied volume of particle i and the total cell volume, ranging between 0 and 1 depending on the partial volume of particle i in the fluid cell. In this study, the divided void fraction method (Nguyen and Indraratna, 2022) is employed to divide the particles into smaller sub-domains with a local centre of mass, resulting in a more accurate calculation of void fraction.

2.3. Particle-fluid interaction

In a fluid-particle system, fluid flowing through a particulate porous medium generally imposes a collection of hydraulic forces on solid particles due to interactions between particles and the surrounding fluid. Following Zhu et al. (2007), the hydraulic forces can be broadly comprised of the drag, pressure gradient and viscous forces, along with other unstable forces such as the virtual mass, the Basset and the lift forces. Among these forces, the drag, the pressure gradient and the viscous forces are the dominant fluid forces acting on the particles (Zhu et al., 2008). Therefore, this study considered the fluid-particle interaction force $\boldsymbol{F_f^i}$ as the sum of the drag $\boldsymbol{F_d}$, pressure gradient $\boldsymbol{F_{\nabla p}}$ and the viscous forces $\boldsymbol{F_{\nabla \bullet \tau}}$ as follows:

$$\boldsymbol{F_f^i} = \boldsymbol{F_d} + \boldsymbol{F_{\nabla p}} + \boldsymbol{F_{\nabla \bullet \tau}} \tag{10}$$

The drag force $\boldsymbol{F_d}$ is primarily attributed to the detailed differences of point stress tensor in the fluid surrounding the particle, while the pressure gradient and viscous forces arise due to the macro-scale stress variations such as the alterations of the fluid stress tensor among various fluid cells. The drag force $\boldsymbol{F_d}$ often accounts for a significant part of the total hydraulic force affecting the migration behaviour of particles. This force heavily depends on the relative velocity between the fluid and the particle, which has been described through various theories (Di Felice, 1994; Tsuji et al., 1993). Kafui et al. (2002) showed that the Di Felice's calculation produces a continuous change in drag force in relation to porosity, which is deemed suitable for a wide range of flow and granular regimes. Therefore, this study employed the Di Felice formulations to approximate the magnitude of drag force as follows:

$$\boldsymbol{F_d} = \frac{1}{8} C_d \rho_f \pi d_p^2 n_f^2 \left(U_f - U_p\right) \left|U_f - U_p\right| n_f^{-\chi} \tag{11}$$

where d_p and U_p are the diameter and velocity of the particle; C_d is the fluid drag coefficient based on the Reynold particle number Re_p as follows:

$$C_d = \left(0.63 + \frac{4.8}{\sqrt{Re_p}} \right)^2 \tag{12}$$

and the Re_p is computed with respect to the viscosity of fluid μ_f as:

$$Re_p = \frac{n_f \rho_f d_p \left|U_f - U_p\right|}{\mu_f} \tag{13}$$

The term $n_f^{-\chi}$ in the Eq. (11) denotes the porosity changes with the presence of other particles in a fluid cell with respect to the correlation factor χ, which is estimated as:

$$\chi = 3.7 - 0.65 \exp\left(-\frac{\left(1.5 - \log_{10} Re_p\right)^2}{2} \right) \tag{14}$$

In addition to the drag force, the pressure gradient force is another major contributor to the total fluid force, especially when the volume of particle (V_p) causes a difference in pore fluid pressure across a surface. The current study adopted Zhou et al. (2010)'s formula to calculate this force as follows:

$$\boldsymbol{F_{\nabla p}} = -(\nabla p \boldsymbol{I}) V_p \tag{15}$$

Moreover, the viscous force is derived from the gradient in the shear stresses across the fluid flowing space as follows:

$$\boldsymbol{F_{\nabla \bullet \tau}} = -\left(\nabla . \boldsymbol{\tau_f}\right) V_p \tag{16}$$

3. Numerical setup

3.1. DEM sampling

The DEM domain was first established to simulate the granular medium before coupling with fluid phase in CFD. In the initial state, fines were not included in the generation of the coarse matrix, but rather introduced at the inlet and subsequently transported by fluid flow to infiltrate into the coarse layer. The coarse particle size distribution (PSD) was initially selected within the range of 1.18 mm to 2.36 mm, following the size of crushed basalts used in granular column experiments conducted by Black et al. (2011). Various coarse size distributions were also considered as shown in Fig. 1 where different size ratios between the coarse and fine constituents were examined as one of the critical factors influencing particle clogging. Given a predetermined PSD, a representative element volume (REV) of coarse particles was generated using a radius expansion procedure to generate a random distribution of skeleton particles. This method is efficient in generating homogenous samples with a specific porosity by adjusting spatial distribution of each particle and expanding particle size effectively (Jiang et al., 2003). The resulting REV of coarse particles was selected to cover a width of 16 mm which was 7–8 times greater the largest particle size and comprised of more than 500 coarse particles. Before adopting this size for subsequent investigations, specimen widths were varied from 16 to 24 mm to evaluate their effects on simulation results. The findings indicated that the selected size of 16 mm wide was sufficient to achieve a representative element volume as there was no significant change in the results regarding infiltration patterns and ratios while increasing the number of particles within periodic cells. Additionally, by using the periodic cell, the simulations can effectively represent an infinite system, thus reducing the need for an excessively large specimen size. This approach allows the replication of interactions across cell boundaries, providing a more accurate representation of real-world conditions while maintaining computational efficiency.

The current study focused on cohesive fines in the forms of particles and/or clusters with the size ranges as shown in Fig. 1. It is noteworthy that while individual clay and silt particles have smaller sizes, they often exist in large clusters in contexts such as soft soil treated by vertical drains and formation of subgrade under rail tracks (Nguyen and Indraratna, 2019; Silva et al., 2023). The small size of fine particles signifies the importance of cohesive attractions such as the van der Waals forces and electrostatic attractions as compared to the body weight of particles under the gravitational effect. Consequently, the consideration of interparticle cohesion via the attractive (cohesive)

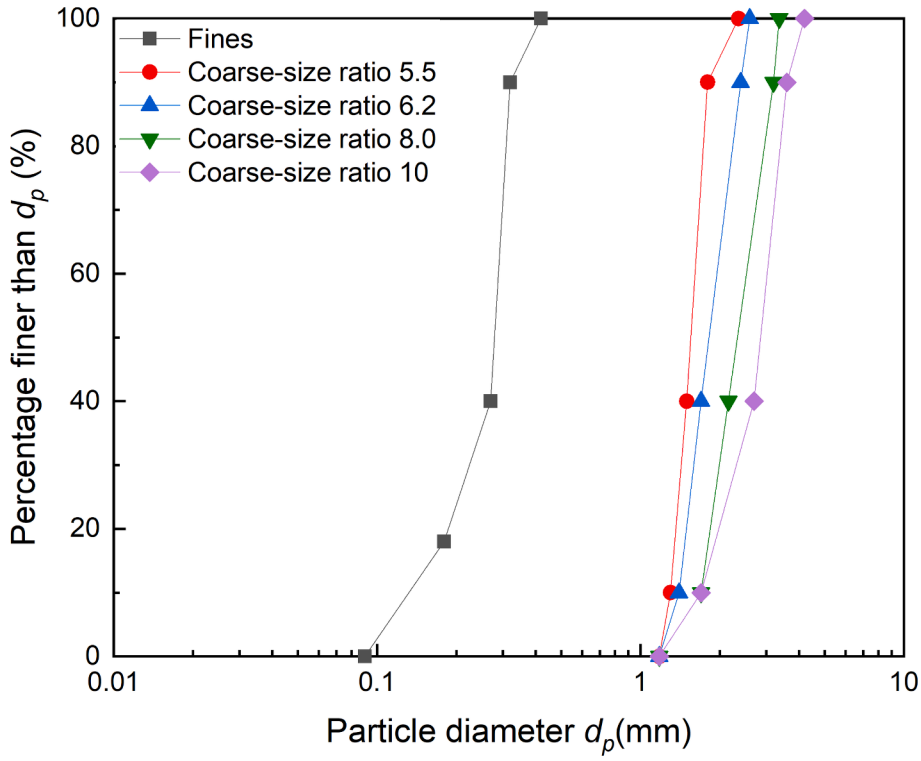

Fig. 1. Particle size distribution of fines and coarse materials with varying size ratio.

force between particles becomes a pertinent aspect of the analysis. In this regard, the concept of Bond number (Bo), which has been extensively used in previous studies (Castellanos, 2005; Singh et al., 2014; Xu et al., 2024), was employed to normalise the magnitude of cohesive force against the particle self-weight. A higher Bond number indicates stronger cohesive forces relative to gravitational effects (Seville et al., 2000). Past study (Vowinckel et al., 2019) determined Bo values in the range of 5–10 for weakly fine-grained soil such as silt. Moreover, Xu et al. (2024) delineated a critical Bo number of 10 beyond which the effect of interparticle attractive forces cannot be ignored. Therefore, in this study, a range of Bo from 0, 5, 10, and 20 was selected to capture the transitional behaviour between cohesionless and cohesive fines. Moreover, the Bo value between coarse and fine particles is selected as unity where the cohesive force is equal to the gravitational force. Previous studies (Vowinckel et al., 2019; Xu et al., 2024) have demonstrated that the case of Bo = 1 is associated with weak cohesion, particularly in interactions between quartz and silt particles. Moreover, Castellanos (2005) identified the case of Bo = 1 as signifying the transition between cohesive and non-cohesive flow regimes where interparticle cohesion just starts to have an observable impact on particle behaviour without being the dominant force. In view of the above, Bo = 1 is adopted in the current study to estimate the cohesive interaction between coarse and fine grains. As a result, the Cohesion Energy Density (CED) values were computed in the range of 0, 1 x 10^4, 5 x 10^4, 1 x 10^5, and 2 x 10^5 J/m^3 to encompass a broad spectrum of cohesive strength of Bo number from 0, 1, 5, 10 and 20 respectively.

In the DEM modelling process, idealised spherical particles were considered in this study to represent the fine and coarse materials, enabling fundamental insights into the migration and clogging process while minimising the number of variables in the computational modelling (Phan et al., 2021). It is acknowledged that while the idealised particle shapes might not fully replicate the complex fluid-soil interactions and pore geometries of angular granular soils, the detailed investigation of particle shape effect is beyond the scope of this study. Additionally, parameters such as Poisson's ratio (ν) and particle density were selected based on measured values of natural granular soil (Zhao and Shan, 2013). For instance, the solid particle density was assumed to be approximately 2650 kg/m^3 to represent the laboratory measurements (Indraratna et al., 2021). Past studies (El Shamy and Zeghal, 2005) have indicated that computational parameters can be reasonably assumed without having a considerable impact on simulation outcomes. Indeed, Lommen et al. (2014) revealed that scaling down of particle stiffness is an effective technique to minimise the excessive computational cost while having a minor influence on the overall behaviour. Other DEM

Table 2
Summary of numerical parameters in CFD-DEM simulations.

Numerical parameters	Inputs	References
DEM parameters (coarse)		
Particle density (kg/m^3)	2650	(Nguyen and Indraratna, 2022)
Particle size (D_s) (mm)	0.9–2.36	
Number of particles	250–500	
Poisson's ratio	0.3	(Derakhshani et al., 2015)
Young's modulus (GPa)	0.1	(Kanitz and Grabe, 2021)
Restitution coefficient	0.2	(Hu et al., 2019; Tao and Tao, 2017)
Sliding friction coefficient	0.3	(O'Sullivan, 2011)
Rolling friction coefficient	0.1	
Gravitational acceleration (m/s^2)	9.81	
Vertical and horizontal pressures (kPa)	20	
DEM parameters (fine)	Inputs	
Particle size (D_f) (mm)	0.09–0.42	
Number of particles	50,000	
CFD parameters	Inputs	
Fluid density (kg/m^3)	1000	(Nguyen and Indraratna, 2022)
Viscosity (Pa. s)	1.004 x 10^{-3}	(Nguyen and Indraratna, 2022)
Fluid cell dimensions (mm)	4 x 7 x 7	
CFD-DEM parameters	Inputs	
DEM Timestep (s)	10^{-6}	
Coupling interval	100	
CFD Timestep (s)	10^{-4}	

parameters such as sliding and rolling friction coefficients were assumed to be 0.3 and 0.1, respectively, which are closely representative of measured values of geomaterials. A summary of these parameters with references is provided in Table 2.

For the boundary conditions of DEM samples, periodic-type walls were used within the coarse region to generate continuous particle interactions across computational walls, thereby minimising the heterogeneous behaviour observed at boundaries. Nguyen and Indraratna (2020) investigated the effect of fixed and periodic boundary types on the CFD-DEM simulations and suggested that the periodic approach offers a more realistic representation of soil materials in the field. Moreover, servo-controlled walls were applied to a top boundary and a left boundary at the fine region with the mean effective stress $p' = 20$ kPa, which aims to mimic the shallow layer of the granular column. The applied load not only acts to strengthen the load-bearing capacity of the soil skeleton, but also compacts the soil sample to cause tighter constriction size of the soil matrix. It is noteworthy that deformation including lateral displacement and dilatancy, often occurs significantly at the topmost region of the granular column, leading to greater interaction between fine soil and granular column. The influence of surcharge loading on the stress behaviour of the soil-column composite was not considered here because this study's primary focus is the influence of interparticle cohesion on particle migration and clogging. A representative DEM sample corresponding to the interface region between the granular column and the surrounding soil is depicted in Fig. 2a while Fig. 2b provides an enlarged view of the selected REV focusing on the interaction between fines and the granular medium under the specified loading conditions.

3.2. CFD procedures modelling fluid flowing through DEM soil

The CFD procedure employs a numerical discretisation technique known as finite volume method (FVM) to partition the CFD domain into smaller computational cells. Within these controlled cells, the averaged fluid variables such as fluid pressures and velocities are computed based on the modified Navier-Stokes equation, accounting for the presence of both solid and fluid phases. For computational efficiency, the size of CFD cells is required to be approximately 2 to 5 times larger than the maximum size of soil particles, following established literature (Kloss et al., 2012). Specifically, the dimensions of the fluid cell in this study were set at 4 mm, approximately twice the size of the largest DEM entities. Moreover, this study modelled a rather small element (REV) focusing on the interaction behaviour between incoming fines and coarse particles at the interface so that the flow direction of this small sample can be approximated as occurring in a single plane (planar). Additionally, the dimensions of the CFD domain were slightly extended at the inlet and the outlet from the DEM region to ensure the well-defined flow path across the granular medium boundaries as shown in Fig. 3a. It is important to note that these meshing conditions remained constant across different simulated scenarios considered in this study to ensure the computational consistency.

In each numerical simulation, the fluid flow was initiated by applying differential pressures (Δp) between the inlet and outlet boundaries of CFD to introduce hydraulic gradients i across the sample length L. Moreover, slip walls were imposed on CFD boundaries to allow fluid flow to slide tangentially along the wall's surface without frictional resistance. For numerical stability, the inlet pressures were incrementally applied while zero-pressure condition was enforced at the outlet boundary as shown in Fig. 3b. This incremental application of i enabled the system to reach a steady state or equilibrium where the simulations can gradually adapt to evolving conditions and potential instabilities. A specific interval of 100 steps was defined in the CFD-DEM coupling, meaning that for every 100 iterations in DEM computations, particle information was transferred to the respective CFD solver. During the simulations, the Courant-Friedrich-Lewy (CFL) number was continuously monitored to remain below unity to ensure computational stability (Kloss et al., 2012). DEM and fluid parameters are also provided in Table 2.

4. Results and discussion

4.1. Sensitivity analysis with varying cell configurations

Before conducting further investigation, a detailed analysis of the flow field with varying CFD cell sizes was conducted to ensure the robustness of our results. The CFD domain, overlapping the DEM domain, was discretised into different combinations of equally sized cells in the x, y, and z directions. Because the flow condition was predominantly in the x- direction (inward the column), the change of cell size was only made in the flow (x) direction while they were kept constant in other directions. Three different mesh discretisation were tested, including 5, 6, and 7 cells (corresponding to fluid cell/maximum particle size = 1.5 to 2.2). Their time-dependent average fluid kinematic pressure and velocity were compared. Our findings indicate that when the ratio between the fluid cell and particle size decreases to a small level (i.e., the case of 7 cells), the fluid velocity becomes deviated from other cases (see Fig. 4). This occurred because the calculated porosity in the fluid cell (using divided void fraction method) became unrealiable when

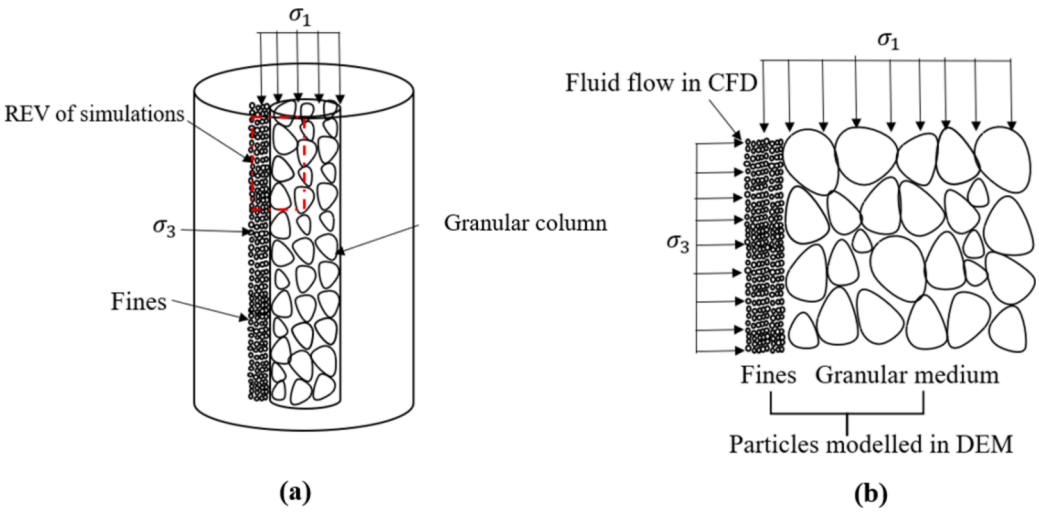

Fig. 2. (a) Schematic of the granular column and fines showing the location of the representative element volume (REV) for simulations. (b) Enlarged view of the selected REV within the granular column under associated loading conditions.

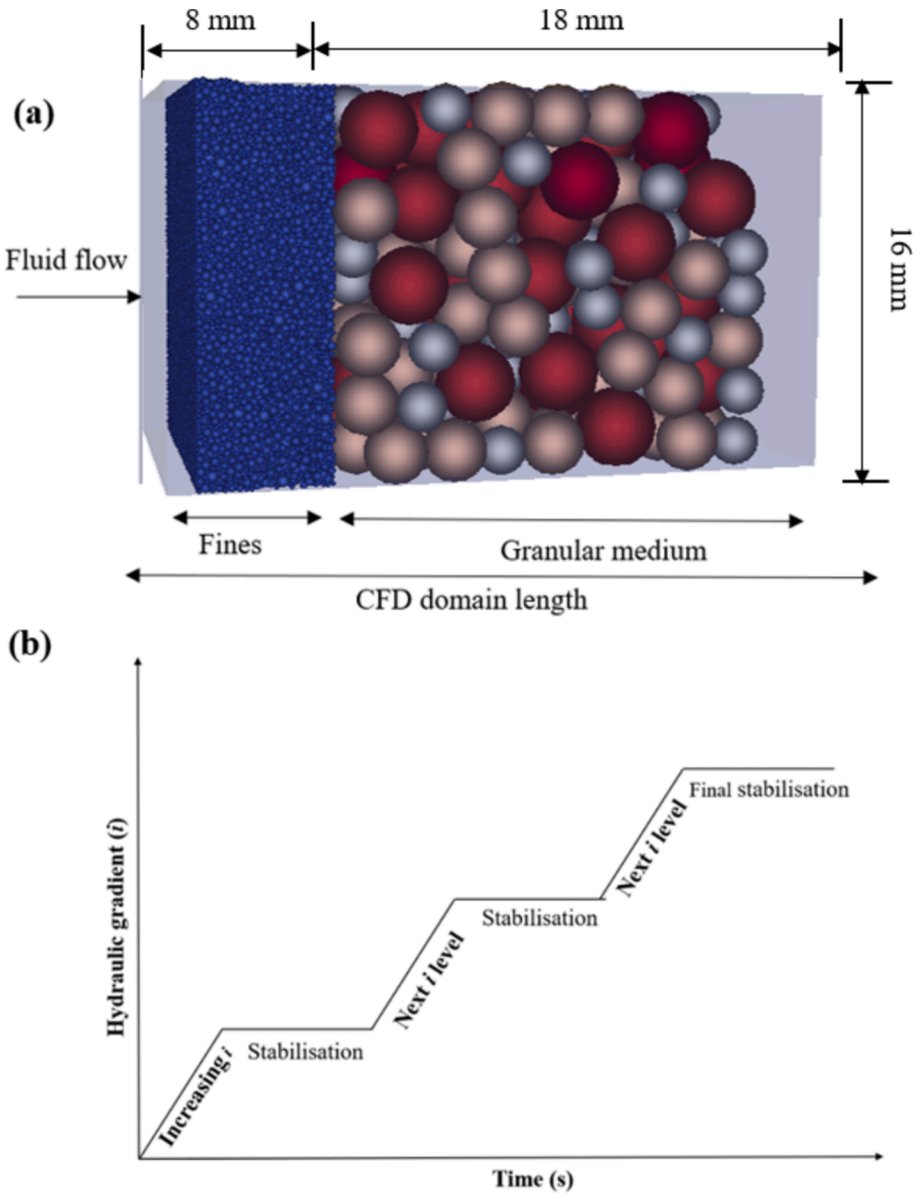

Fig. 3. a) coupling cfd-dem modelling of the soil-column interface and b) hydraulic loading process.

the ratio of fluid cell/particle size is small, resulting in inaccuracies in the fluid velocity computation. The investigation proved that the adopted mesh configuration (6 cells in the flow direction) provided a good balance between computational efficiency and accuracy.

4.2. Validation of CFD-DEM results with analytical results

Before the current CFD-DEM simulation was used to investigate the microscale interactions between fine and coarse particles in filtration and clogging, it is essential to validate this method with existing solutions. A semi-empirical approach based on the modified Kozeny-Carman (KC) equation was thus adopted to estimate the hydraulic behaviour, and the results were used to compare with the coupled CFD-DEM outcomes. The KC equation is widely employed to estimate the pressure drop and flowing velocity of a fluid in porous media (Carman, 1937). However, this equation is formed based on an assumption of a laminar flow in homogenous granular medium, making it relevant mainly to systems with uniform particles and low Reynolds numbers. Ergun (1952) introduced an extension incorporating viscous and inertial forces following the KC equation. The resulting Ergun equation applies to a broader range of flow regimes and conditions, accommodating laminar and turbulent flows. Consequently, it has become one of the most renowned correlations for predicting pressure drop and flow condition in fluid mechanics. In this study, the CFD-DEM results on pressure drop and flowing velocity are compared with the results from Ergun equation shown as follows (Erdim et al., 2015):

$$\frac{\Delta p}{\Delta L} = 150\frac{(1-\eta_f)^2 \mu V_s}{\eta_f{}^3 d_p^2} + 1.75\frac{(1-\eta_f)\rho_f V_s^2}{\eta_f{}^3 d_p} \tag{17}$$

where Δp is the pressure variation across the bed length ΔL; V_s is the superficial velocity determined at the empty cross-section of the bed; ρ_f and η_f are the fluid density and viscosity, while d_p is the particle diameter. It is noteworthy that the pressure variations Δp were taken along the horizontal axis of the simulated column.

For the comparison of hydraulic behaviour predicted by the numerical and analytical methods, the case with size ratio of 8 was used for calculation. The required parameters such as the pressure drop, porosity and particle sizes of the coarse region were used to calculate the V_s using the Ergun equation (Eq. (17)), whereas the numerical velocity of fluid

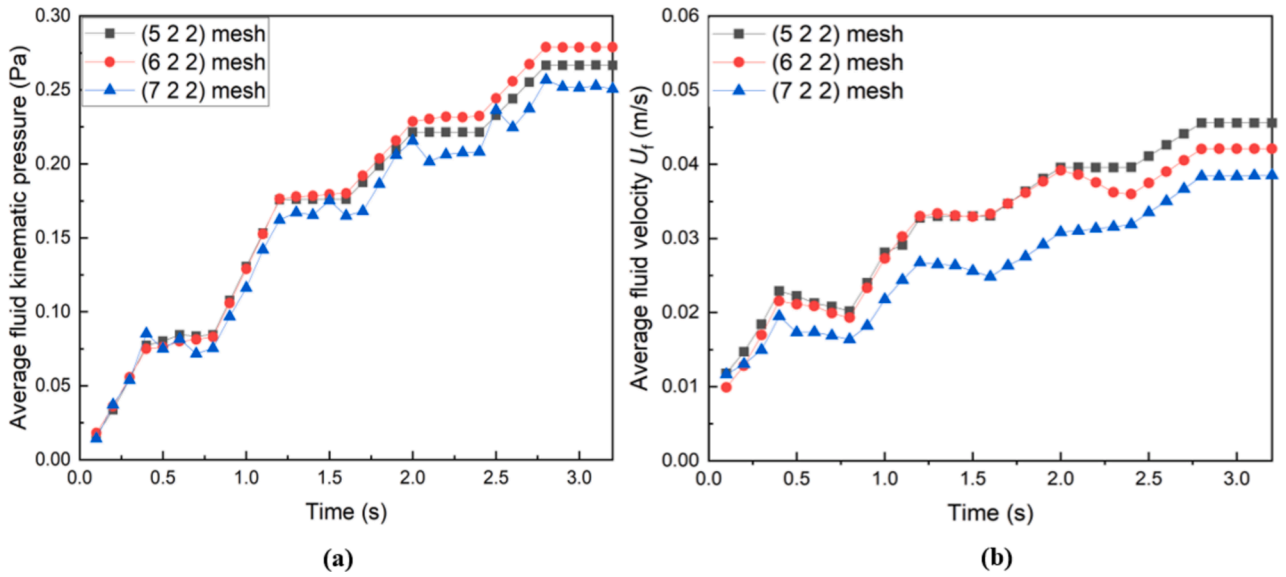

Fig. 4. Flow field analysis with varying CFD cell configuration in terms of a) fluid pressure and b) fluid velocity.

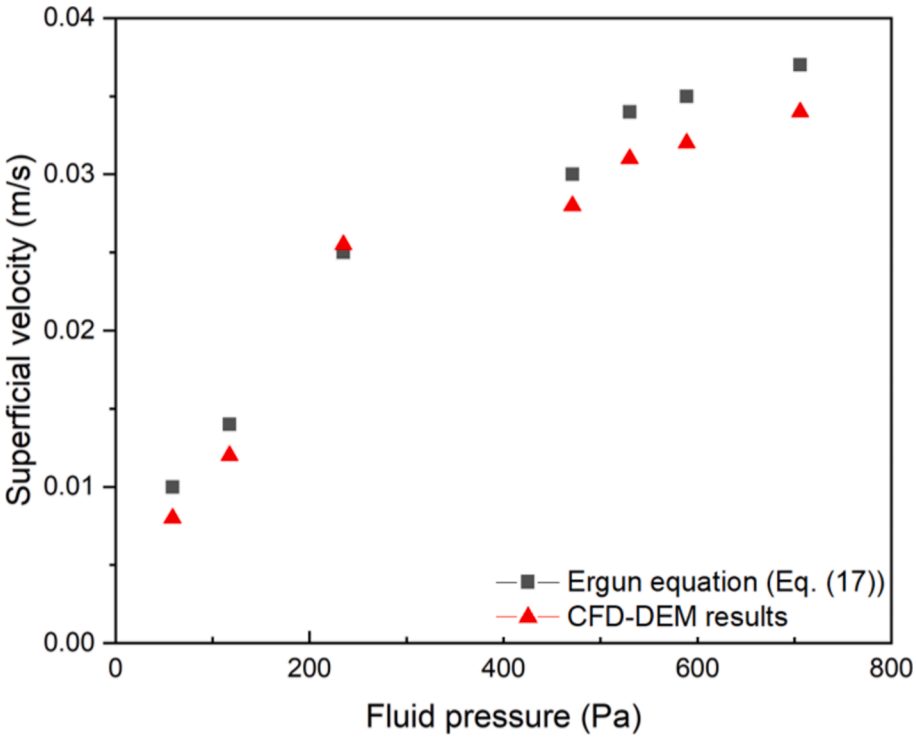

Fig. 5. Relationship between superficial velocity and pressure predicted by CFD-DEM model compared to analytical (Ergun) method for the case with size ratio of 8.

flow at the corresponding region was numerically calculated from CFD-DEM computation for comparison based on the modified Navier Stokes equations (Eq. (8)). Note that the Reynold number of fluid flow was also monitored to ensure that the flow condition remained laminar ($Re < 10$). The results of fluid velocities predicted by these two methods at different pressure levels are shown in Fig. 5, which indicates a good agreement between the conventional Ergun solution and CFD-DEM coupling. Despite varying pressures used, the deviations between the two methods across different points are less than 5 % of the velocity magnitude, attesting to the accuracy of CFD-DEM simulations. The discrepancies are inevitable due to the fact that the idealised Ergun equation might not fully encapsulate the complex fluid-particle interactions occurring when fluid continuously flows through the granular medium.

4.3. Preliminary investigation on the migration and clogging behaviour of cohesionless particles

A benchmark investigation was conducted on cohesionless fines flowing through the porous media that helped establish a standard case based on rigorous understanding of the filtration response of cohesionless soils in literature. In this analysis, the size ratio between fine and coarse particles varied from 5.5 to 10, and the filtration behaviour was observed under the same hydraulic flow where the hydraulic gradient is incrementally increased with time reaching $i_{max} = 3$. Fig. 6 shows

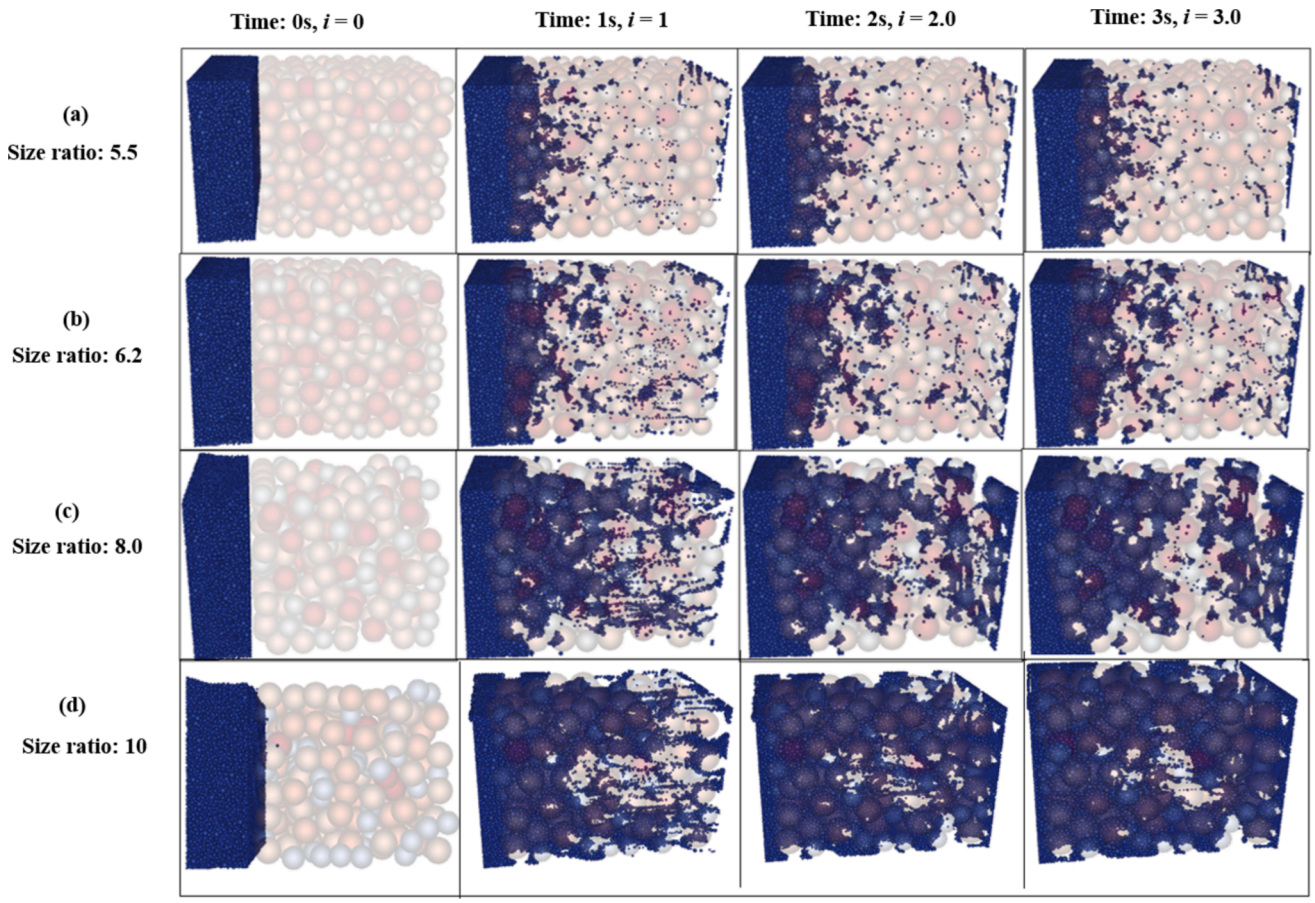

Fig. 6. Migration and clogging of cohesionless fine particles with different size ratios.

different migration patterns of cohesionless fines through porous media considering different geometric size ratios. Two stages can be identified, (*i*) coarse particles expand under the applied vertical load and intrude into the fine region, and (*ii*), loose fine particles are increasingly squeezed into interconnected voids within the granular bed under increased hydraulic forces as shown in Fig. 6. When comparing the migratory behaviour of fines across different size ratios, the extent of fine infiltration significantly increases when the size ratio increases from 5.5 to 10. When the size ratio is small such as 5.5–6.2 as shown in Fig. 6, most fine particles are retained at the interface region of the granular column despite the hydraulic gradient continuing to increase. However, when the size ratio ≥ 8, a massive migration of fines through the course medium can be observed.

The above process can be further assessed through a quantified parameter called infiltration ratio, which reflects how well the suspended fine particles are capable of infiltrating into the coarse medium under the influence of fluid (Kim and Whittle, 2006; Prempeh et al., 2020). The infiltration ratio is defined as the mass quantity of fine particles flowing into the granular column to the total mass of fines released from the inlet. Fig. 7 clearly shows that when the size ratio is marginal such as 5.5 and 6.2, the infiltration ratio only increases modestly at the beginning when fines mostly infiltrate and significantly reduce the pore spaces near the interface of the coarse column. This process leads to the formation of a clogging zone, which acts as a physical barrier to prevent further infiltration of fines. As a result, the infiltration ratio only increases to around 19 % at early stage (after 0.25 s) then becomes stabilised even though the hydraulic gradient continues to rise. However, when the size ratio exceeds 8, the infiltration ratio increases substantially, leading to the accumulation of over 50 % and 80 % fine particles in the granular medium at the end of simulations. In fact, with increasing size ratios (>8), the coarse medium almost loses it retention capacity so that majority of fines can migrate through its porous system easily. These findings align with the previous filter design observations (Foster and Fell, 2001), which experimentally determined that a size ratio of 7 marked the upper limit of no erosion, whereas a size ratio of 9 indicated the lower limit of continuing erosion.

Moreover, our numerical results were compared with existing experimental data for further validation, primarily focusing on cohesionless fines due to the availability of extensive experimental results in this area. Fig. 8 presents a comparative analysis between CFD-DEM results and experimental data from (Gibson et al., 2010) in terms of the concentration of infiltrated particles along the length of granular medium (L). It shows when size ratio is small (6.2), over 30 % of interstitial fines by weight are concentrated in the shallowest layer (l = 0) while a significant drop in fine content (less than 5 %) is observed at the farthest distance from the inlet. However, when the size ratio increases to 10, the coarse medium allows for unimpeded infiltration profiles, meaning that the infiltrated fine content is uniformly distributed throughout the sample thickness. This comparison confirms the accuracy of the numerical approach for cohesionless fines. However, due to the scarcity of relevant experimental data on cohesive fines, further experimental work is still necessary to validate the numerical results for these materials.

4.4. Migration and clogging behaviour of cohesive particles

Following the preliminary examination of the migratory behaviour of cohesionless particles, this section explores how the migration patterns of fines can change when the interparticle cohesion is included. With the major focus on the influence of cohesion, the size ratio of 8.0, where there is a significant migration of fines (Fig. 6), was selected and remained unchanged through different cohesion degrees. The results (Fig. 9) show considerable influence of interparticle cohesion on the

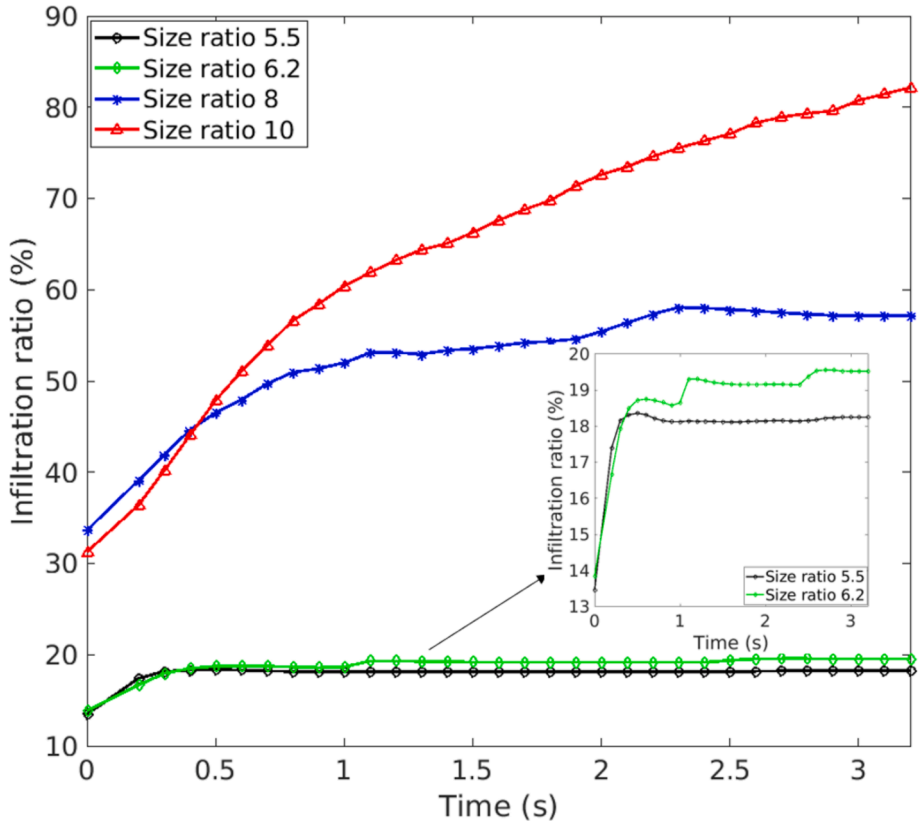

Fig. 7. Evolution of infiltration ratios with increasing size ratios (from 5.5 to 10).

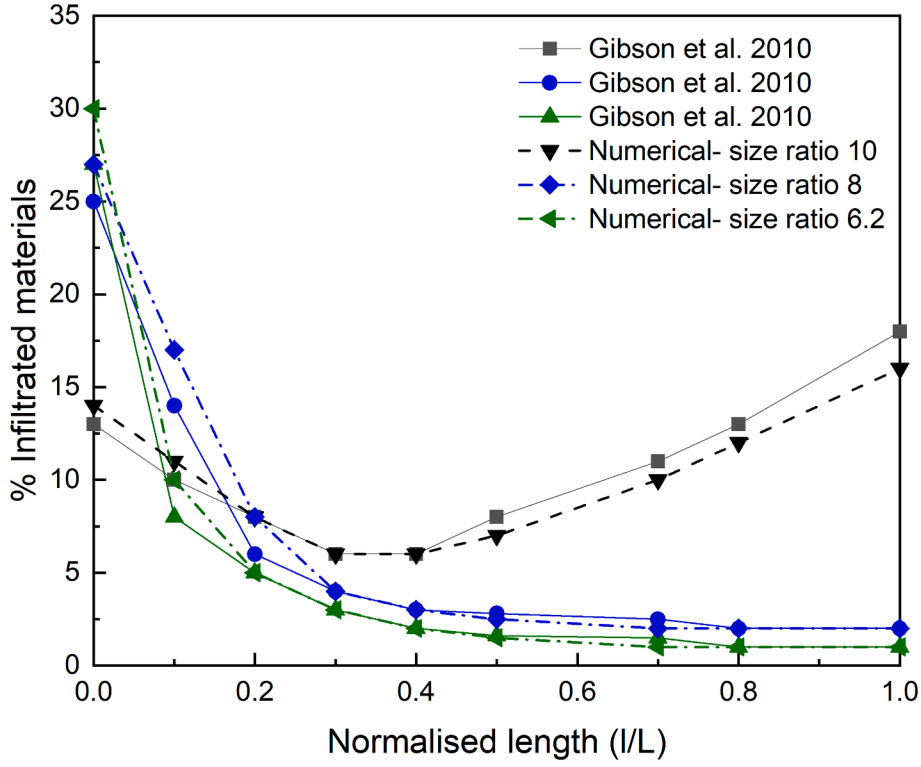

Fig. 8. Validation of numerical simulations for the spatial arrangement of infiltrated fines with varying size ratios, compared with experimental study (Gibson et al., 2010).

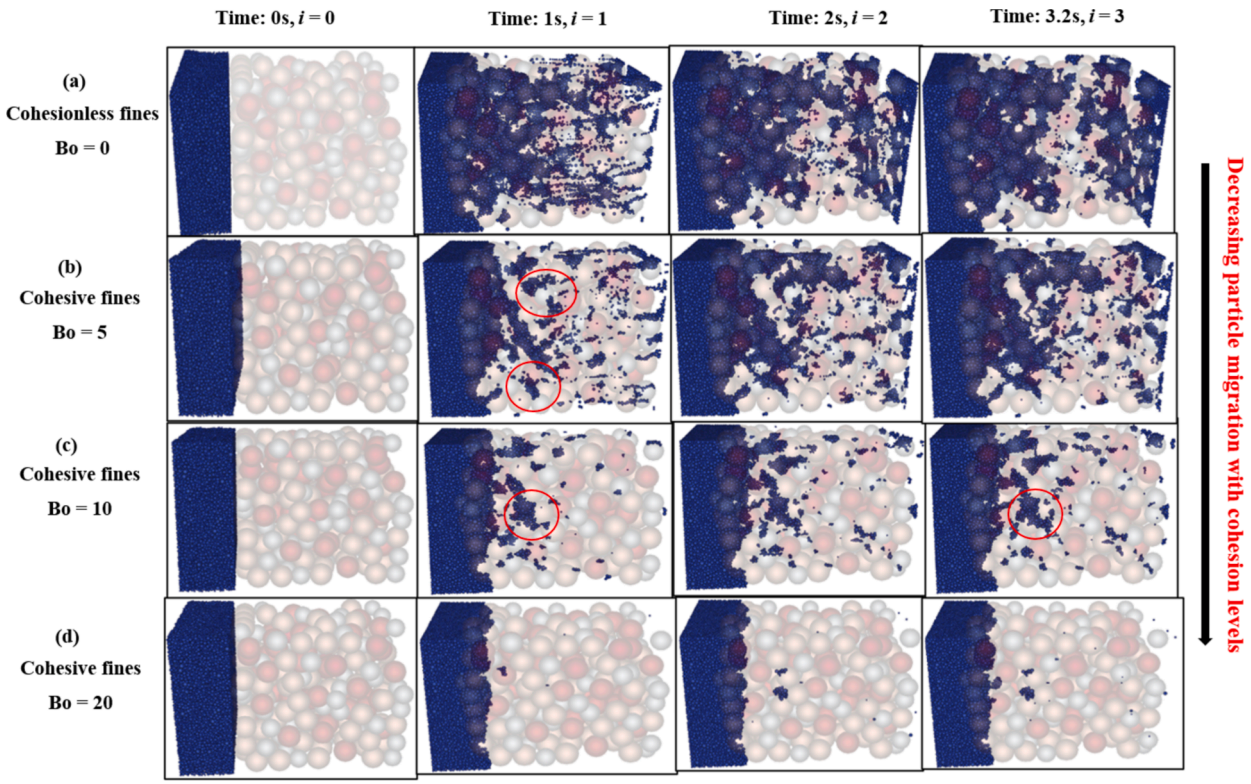

Fig. 9. Visualisation of the migration and clogging behaviour of cohesive particles.

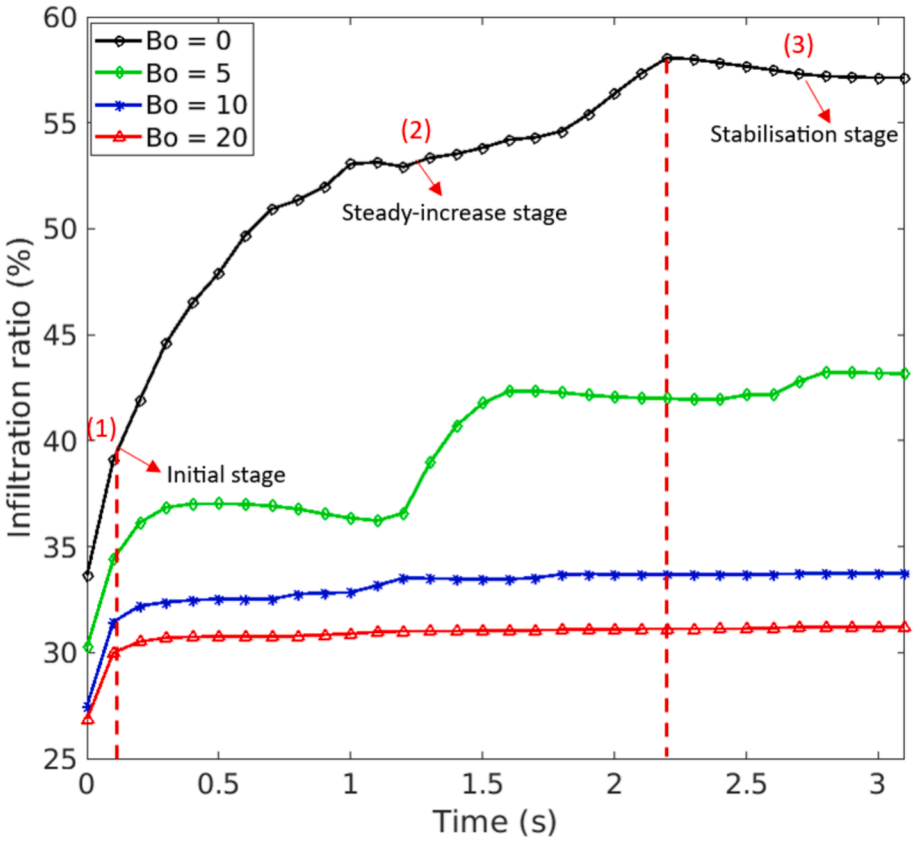

Fig. 10. Change of infiltration ratio patterns with time when cohesion degree (Bo) increases from zero (cohesionless, Bo = 0) to highly cohesive soil (Bo = 20).

clogging development of the fine-coarse interface under horizontal flow. When there is no cohesion or the cohesion is very small, fine particles interact with the coarse matrix mainly through collisional and frictional contacts. By the end of the simulations, a considerable quantity of fines is broadly distributed amongst the voids within the granular assembly. Different from non-cohesive particles, cohesive soil such as small-sized silts and clays exhibit a distinct behaviour due to interparticle attraction forces as represented through the Bo numbers. With the inclusion of cohesion, particle migration is considerably impeded, and where migration occurs, particles tend to form agglomerates or clusters with larger effective sizes, as indicated by the red circles in Fig. 9. Especially, when the Bo number exceeds 10, cohesive fines predominantly accumulate at the interface between coarse and fine materials. This accumulation acts as a barrier to restrict further infiltration of incoming particles, leading to early occurrence of clogging.

Furthermore, with the presence of cohesion, the entire infiltration process can be characterised into three distinct phases: initial infiltration, steady increase and stabilisation as shown in the Fig. 10. For the initial infiltration stage, the cohesionless system undergoes a steady-increase stage where the rate of fine infiltration continuously rises and reaches a final infiltration ratio of 57 %. By contrast, when cohesive force is present and relatively small, the infiltration curve becomes non-smooth (stepwise) and indicates a *meta*-stabilisation stage of clogging as shown in the green line. For example, when Bo = 5, the infiltration ratio becomes stable over the first 1.2 s before rapidly ascending under a larger hydraulic force. This can be seen in the real contexts where silt particles are predominant with very limited amount of clays, the bonds between fines are weak and vulnerable to fluid flows. With further increase in the Bo number exceeding 10, the initial infiltration phase quickly reaches the state of stabilisation within the first 0.5 s, without undergoing through the steady-increase stage. This early stabilisation suggests that increasing cohesion hinders infiltration of particles despite increasing hydraulic gradient with time. When Bo is increased from 5 to 20, the susceptibility that fine particles can infiltrate into the granular column greatly diminishes, reaching final infiltration ratio of approximately 43 % and 31 %, respectively.

Moreover, the instantaneous infiltration ratio curve could serve as an indicator to differentiate between clogging and migration states of fines. Clogging is identified when the infiltration ratio curve reaches a plateau despite continuous flow, indicating that the migration of particles is significantly impeded. Conversely, migration state is characterised by a steady or increasing particle infiltration, showing that particles or groups of particles are still migrating through the pore spaces under the influence of fluid forces. Additionally, this macro-scale observation is supported by estimating velocities of individual particles in DEM. In a clogging state, most of particle velocities drop significantly and become quasi-static (< 0.00005 m/s) though fluid continues to flow, they are thus considered as "static". As shown in Fig. 11, the clogging state which is prevalent in the case of cohesive fines (i.e., Bo = 10), more than 90 % of static particles are obtained and stabilised after 1.8 s, hence the term "most of particles" is used. However, as the hydraulic gradient is increased over time, the percentage of static particles begins to fluctuate slightly, signifying the occurrence of particle remobilisation. Conversely, in a clustering (migration) state which is observed in the cohesionless state (Bo = 0), only less than 10 % of static particles are obtained and fluctuated significantly with higher hydraulic forces. This means a majority of particles still maintain sufficient velocities under influence of fluid flow to move through the granular pores.

The visualisations presented above are consistent with previous experimental and analytical studies on stone column-soil interactions (Basack et al., 2018; Indraratna et al., 2013; Tai et al., 2017), where the intrusion of cohesive fines has led to the formation of a clogged zone starting at the soil-stone column interface, accompanied by a reduction in effective drainage area called unclogged area. In the current study, the clogged region is defined as most fines have lost their kinetic energy and became immobilised at the coarse–fine interface. To facilitate quantitative understanding of localised clogging, the position and distribution of static particles (i.e., defined as particles having velocities less than 0.1 % of the flow velocities) are monitored over the length of the granular medium (as shown in Fig. 12). It shows that the localised clogging or clogged region can be observed at the inlet region where the cumulative percentage of static particles exceeds more than 80 %, hence the term "most fines" is used (Fig. 12a and Fig. 12b). Consequently, the unclogged region is identified as the area where fines are mobile and

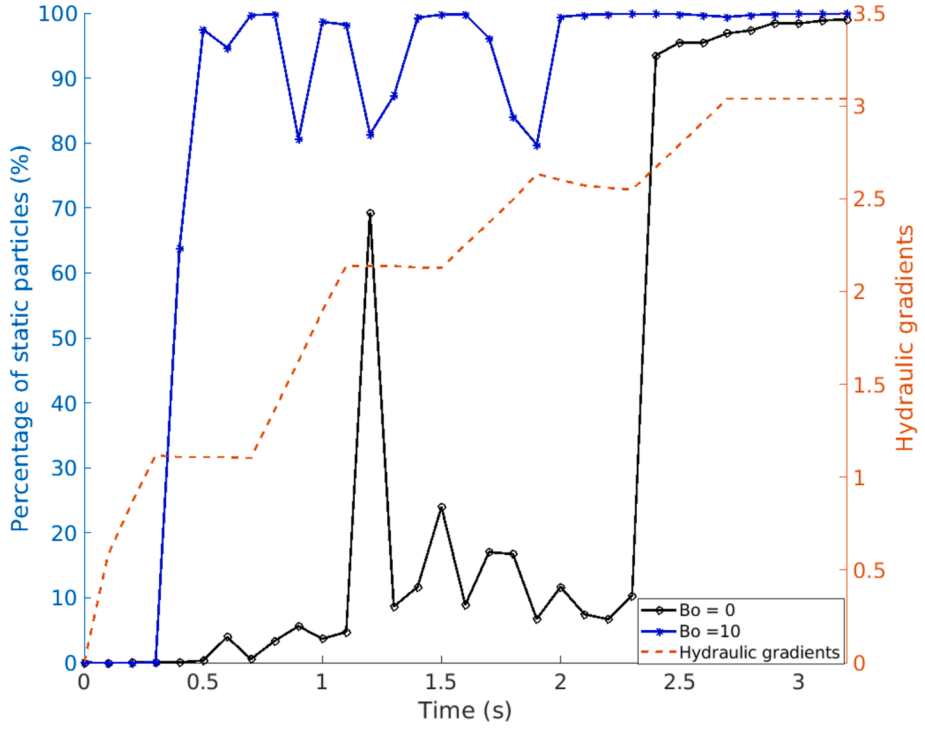

Fig. 11. Percentage of static particles in the clogging state (Bo = 10) and migration state (Bo = 0) varying with time and hydraulic gradients.

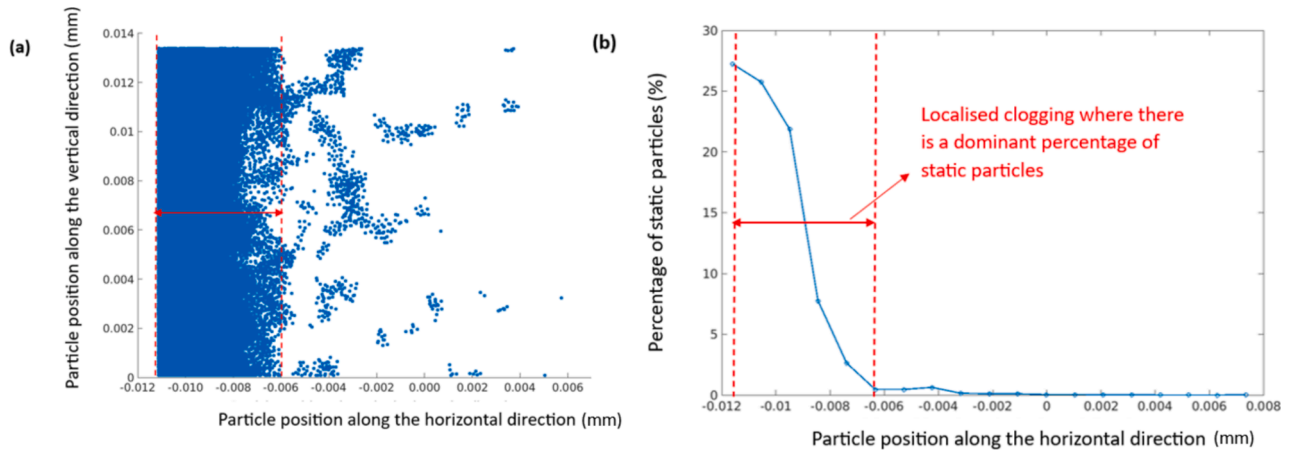

Fig. 12. (a-b) Observation of clogged region based on the position and distribution of static particles (Bo = 10).

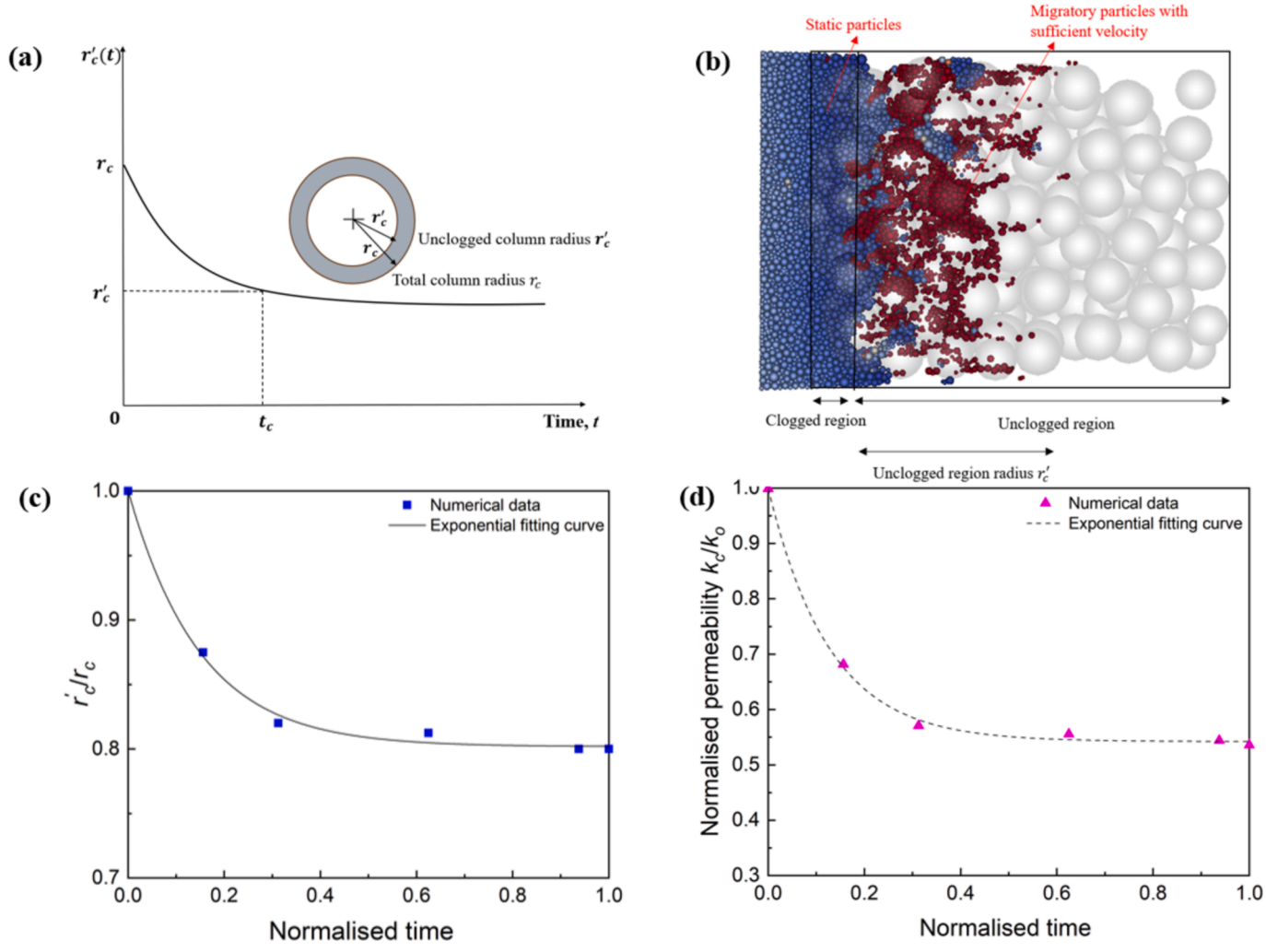

Fig. 13. a) qualitative assumption of clogging parameters with time inBasack et al. (2018), and b) determination of clogged and unclogged region in DEM model, and c-d) time-dependent variation of clogging parameters (i.e., unclogged radius and clogged permeability) in CFD-DEM simulations.

continue to move with sufficient velocity through the pores of the porous media without significant blockages.

Furthermore, a past study (Basack et al., 2018) hypothesised an empirical clogging parameter to describe the radius of the unclogged column zone (r_c') as a function of time (r_c'(t)) as depicted in Fig. 13a. The estimation of clogged and unclogged region in the CFD-DEM simulation is provided in the Fig. 13b. For example, the unclogged radius r_c' is compared with the initial column radius r_c in the case of highly cohesive fines when Bo = 10, and the resulting characteristic curve of the ratio (r_c'/r_c) over time is found analogous to the approach and associated

assumptions elucidated by Basack et al. (2018) (Fig. 13c). Moreover, the clogging parameter α, which can be estimated from α_i, α_f, α_t and T_r' as non-dimensional clogged parameters and assumed time factor proposed in Basack et al. (2018) was found to be approximately 0.96. This corroborates well with the experimental range (0.9–0.94) documented in the same study.

A significant contribution of the present study also lies in monitoring both the rate and extent of the clogging process through the unclogged radius, enabling accurate determination of the critical time (t_c). It is noteworthy that the critical time was proposed in some previous studies to define a threshold at which the clogging process stabilises (Tai et al., 2017), but they were not able to quantify the time-dependent clogging process and delineate a corresponding characteristic value to represent clogging at a given time. By examining the time-dependent curve of the unclogged radius, the current numerical study resulted in a value of t_c at around 30 % of the total time, at which the unclogged zone constitutes approximately 80 % of the original column radius. In addition, the influence of clogging can be evaluated by examining changes in permeability k, typically calculated using Darcy's law ($\frac{\Delta P}{L} = \frac{\gamma_w U_f}{k}$). The variations in permeability within the granular column are represented by the ratio between the permeability of the clogged zone (k_c)) and that of the clean (original) column (k_o), as illustrated in Fig. 13d.The results show that at the critical time ($t_c = 0.3$), the clogged permeability drops about 50 % its initial value after which the reduction becomes marginal over time. This finding again highlights the substantial impact of clogging on the column's drainage capacity at the critical time t_c, and the importance of establishing an accurate and reliable method to quantify this parameter in practical design situations.

4.5. *Localised distribution of infiltrated fine particles within the granular medium*

In the prediction of clogging, previous experimental and analytical studies (Lippera et al., 2023; Locke et al., 2001) identified some significant challenges in determining the characteristic depth that fine particles can penetrate and accumulate, as well as comprehending the spatial distribution of fine particles within the profile of porous media. These insights are crucial for assessing how fast and up to which level the porous column will be adversely affected by clogging. By using the CFD-DEM technique, a detailed understanding of how fine particles are transported into and deposited within the granular medium can be simultaneously obtained. For example, Fig. 14 presents the localised distribution of cohesionless fines within the granular column, which was partitioned into three sections: section A, B and C along the direction of fluid flow. It reveals that the deposition of infiltrated particles is largest at the inlet region (A), followed by regions B and C, and this can be attributed to the higher fluid pressure at the inlet compared to other deeper regions.

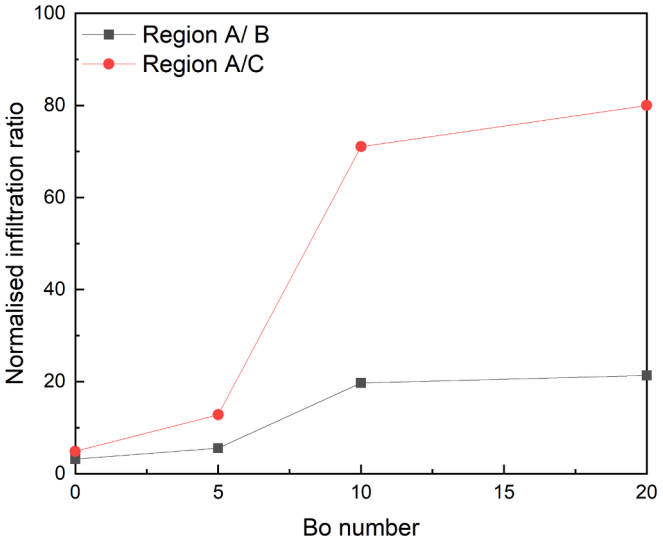

Fig. 15. Localised infiltration ratio with different cohesion levels.

Furthermore, Fig. 15 depicts the variations of infiltration ratios in the region A normalised with region B (black line) and region C (red line) when interparticle cohesion is incorporated by varying Bo numbers. When the cohesion level is increased, the normalised infiltration ratios substantially increase in both cases. For instance, with sufficient cohesion (Bo = 10), the normalised infiltrated ratio between regions A and B reaches a factor of 20, while the ratio between regions A and C escalates to a factor of 70. It highlights that the presence of cohesion exacerbates the retention of particles in the interface region (A), while further impeding the migration of cohesive fines towards deeper regions (B and C). This numerical finding aligns with prior experimental investigations (Zhang et al., 2023) where the presence of liquid cohesion was found to

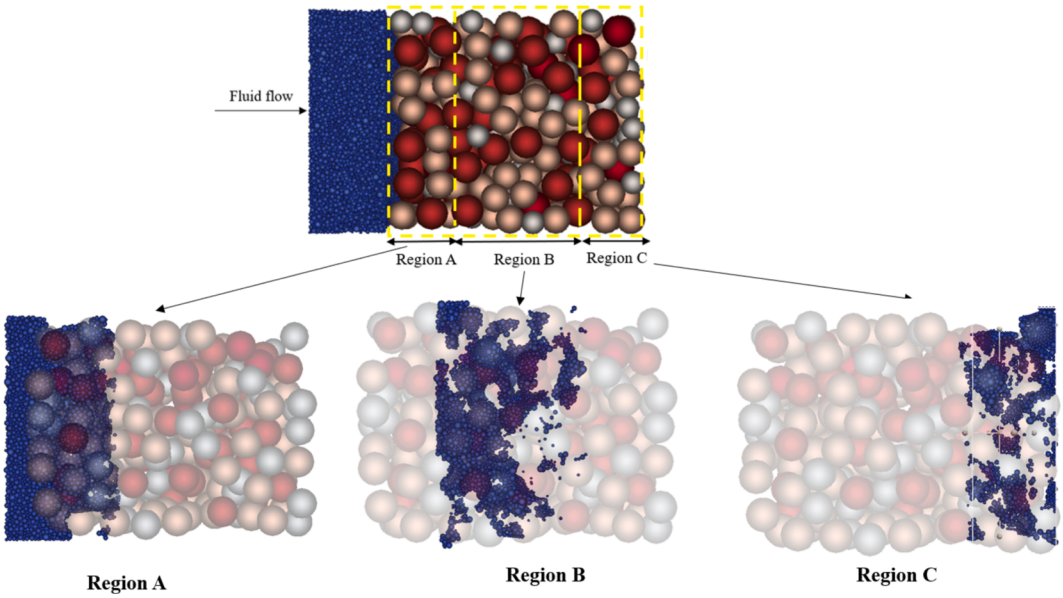

Fig. 14. Localised distribution of infiltrated cohesionless particles throughout the granular medium.

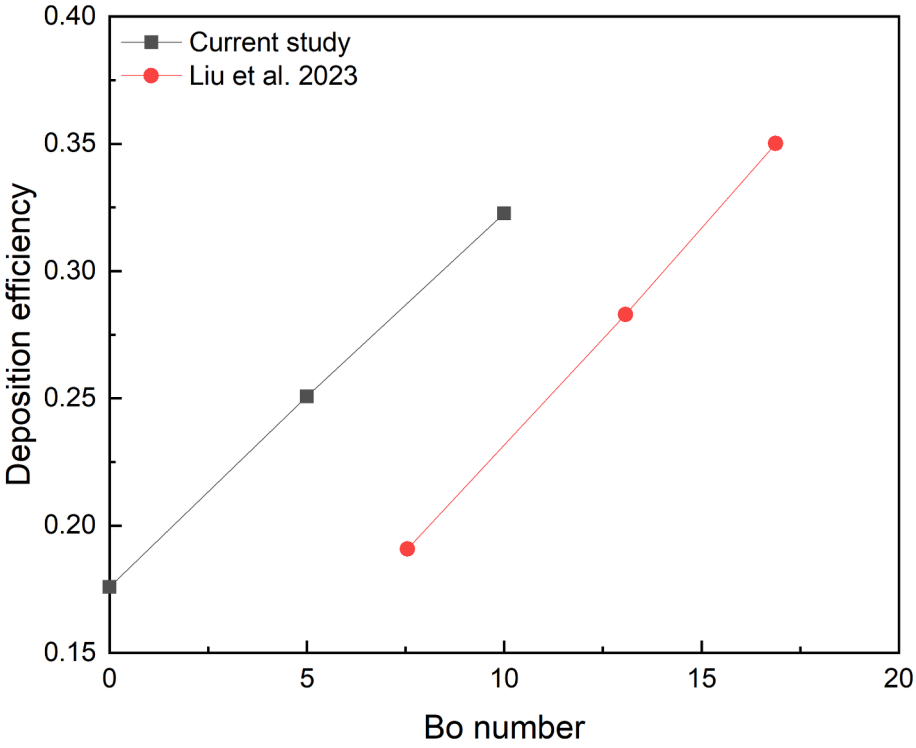

Fig. 16. Deposition efficiency versus cohesion level at the surface region A.

promote significantly the retainment of particles and eventually cause large-scale blockage.

For further analysis, a parameter termed deposition efficiency is quantified as the ratio of the number of deposited particles in the surface region (A) to the number of particles released at the inlet (Elrahmani et al., 2023; Mesticou et al., 2016). This region is critical to further study because it is highly susceptible to clogging due to the high influx of fines released from the inlet (Parvan et al., 2020). The deposition efficiency for various cohesion levels is shown in Fig. 16 demonstrating that the deposition efficiency increases nearly linearly with the cohesion levels. This implies that as the cohesive forces between particles increase, so does the likelihood of particles being deposited within the porous

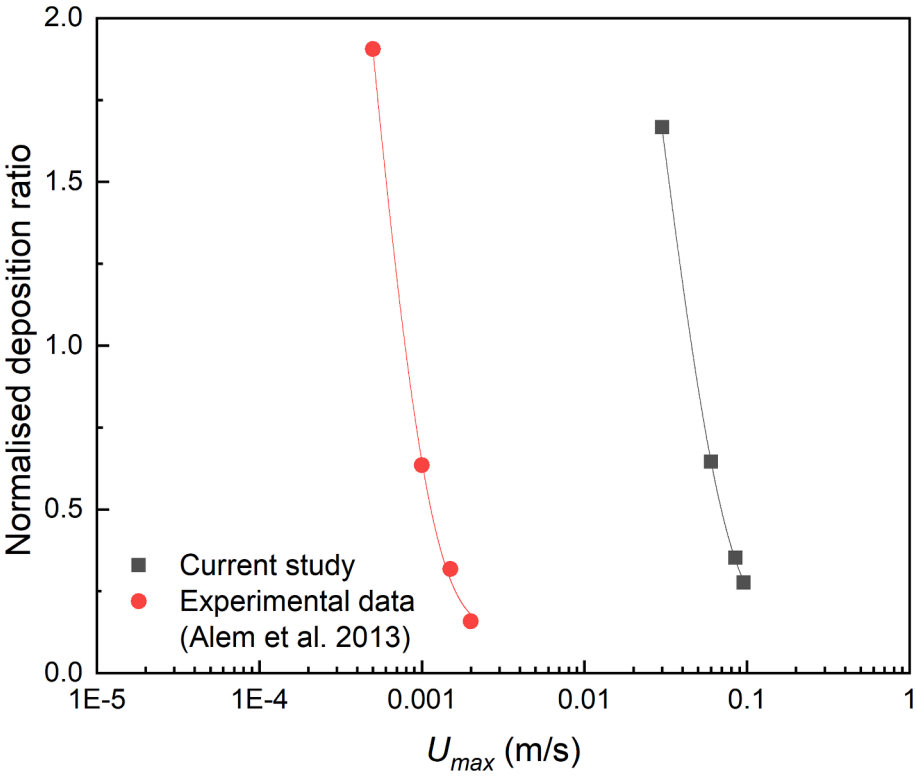

Fig. 17. Deposition ratio as a function of flowing velocity in the current and experimental studies on cohesive Kaolin fines (Alem et al., 2013).

medium. Consequently, incoming particles are more likely to be intercepted by the deposition, which is responsible for accelerating the clogging process. The observed trend is comparable with prior research conducted on a simplified two-dimensional sand matrix (Liu et al., 2023); however, discrepancies inevitably emerge from the use of different fine and coarse materials between the current and past studies.

Further effort has been made to validate our cohesive model by relating our numerical prediction of deposition efficiency over varying flow velocities in contrast to a previous experimental study (Alem et al., 2013). For a consistent comparative analysis, a normalised deposition ratio was used where deposition efficiency was normalised against the coarse–fine size ratio and maximum fluid velocity. Fig. 17 shows that as the flow velocity increases, the ability of fine particles to remain within the fabric of the porous medium decreases, mainly due to the higher fluid drag forces acting on the fines. This trend is consistent with the deposition behaviour of kaolinite particles considered by Alem et al. (2013), which states that higher flow velocities lead to the remobilisation of previously deposited particles, reducing the overall likelihood of deposition. Additionally, the relationship between the deposition ratio and the flow velocity follows a power-law trend, which has been observed in both the current study and prior experiments (Alem et al., 2013; Bennacer et al., 2022). It is also noted that the experimental study (Alem et al., 2013) used finer soil in their experiment, resulting in smaller flow velocity and thus the deviation from the current numerical modelling. By validating the deposition efficiency under both varying Bond numbers and flowing velocities, this study provides an acceptable and convincing comparison with experimental data while strengthening the reliability of the simulations.

4.6. Effect of varying pore geometry on clogging of cohesive fines

It is well established that pore structures of a medium determine the flow paths for fine infiltration, which means fine infiltration is likely to occur when the characteristic throat size or constriction size is larger than a certain proportion of fines. Constriction size refers to the smallest openings or narrowest passages within a porous medium that fines must navigate through. Previous studies (Indraratna et al., 2007) have found that CSD, rather than the PSD governs the infiltration behaviour of a fine-coarse system. In this study, the CSD profile was computed based on a mathematical model examining the densest and loosest particle arrangements of a given particle size distribution (Indraratna et al., 2007). In this mathematical computation, the actual constriction size D_c for any given relative density R_d is given by:

$$D_c = D_{cD} + P_c(1 - R_d)(D_{cL} - D_{cD}) \tag{18}$$

where D_c is the constriction size for a given value of the percent finer P_c; D_{cD} and D_{cL} are the constriction sizes based on densest and loosest packing arrangements. By incorporating these theoretical concepts into a comprehensive computer subroutine, the evolution of CSD curve undergoing the infiltration of fine particles was determined. Indeed, the ratio of mean constriction size (D_c^m) and the accumulated volume of infiltrated particles (V_{pa}) reflects very well the deposition efficiency based on particle volume. The results (Fig. 18 below) show that the larger the ratio D_c^m/V_{pa}, the less the potential of clogging, thus the smaller the deposition ratio. By contrast, when the Bo number increases, the accumulation of cohesive fines (V_{pa} increases) becomes larger, which corresponds to the reduction of mean constriction size and higher deposition ratio. In other words, the clogging potential becomes more significant as the available pore spaces decrease relative to the particle volume.

Moreover, a detailed investigation of how pore structure evolves under the influence of clogging was examined. As the distribution of fines is not uniform, the average constriction size is used here for the inlet region (region A) and it is normalised with the original average constriction size prior to particle infiltration. Fig. 19 analyses the permeability drop in conjunction with the reduction in average constriction sizes at the end of the simulation. The result shows that as the constriction size diminishes, the pathways for fluid flow become increasingly restricted, leading to a noticeable decrease in permeability. This trend is particularly pronounced in cases involving highly cohesive fines (Bo = 20), where the accumulation of particles at the constrictions results in the most significant reduction in constriction size and consequently the steepest decline in permeability.

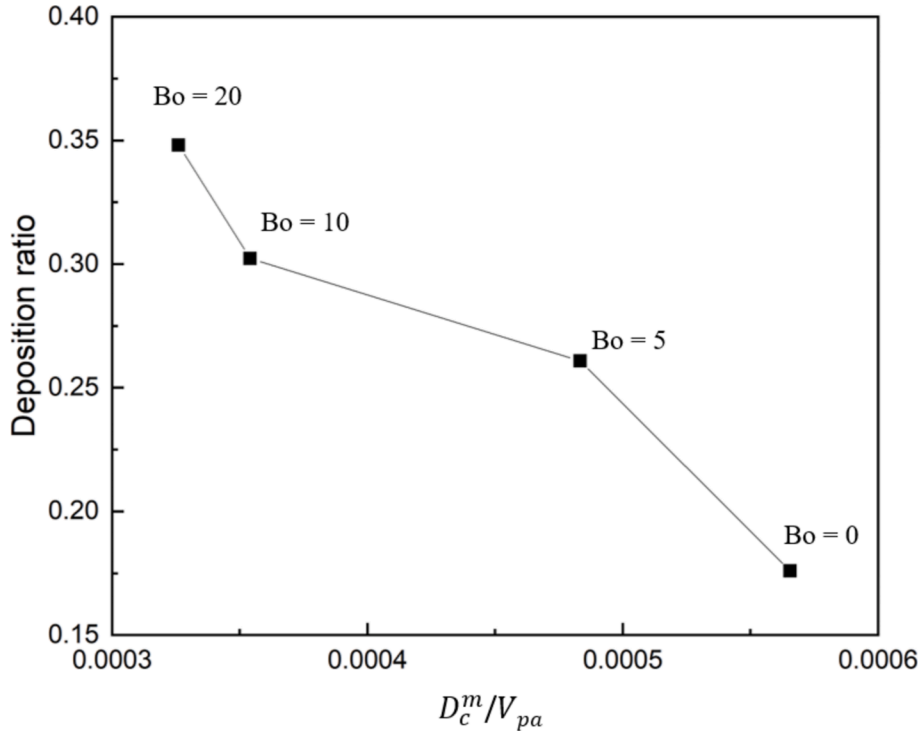

Fig. 18. Relationship between the average constriction size and accumulated particle volume with deposition ratio..

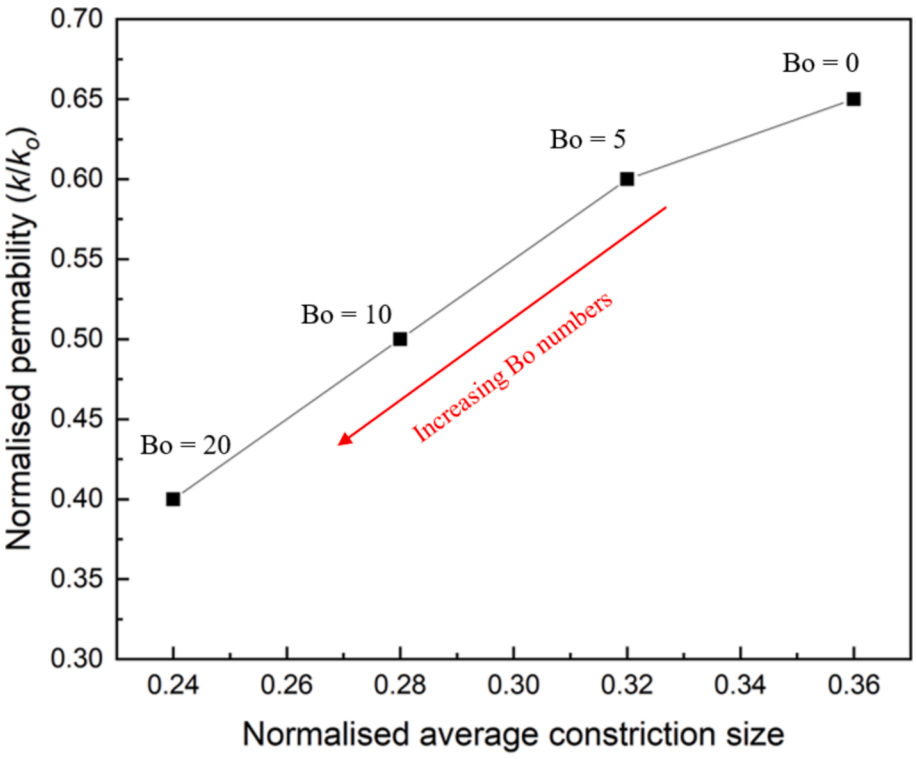

Fig. 19. Relationship between pore constriction and permeability reduction with the evolution of clogging.

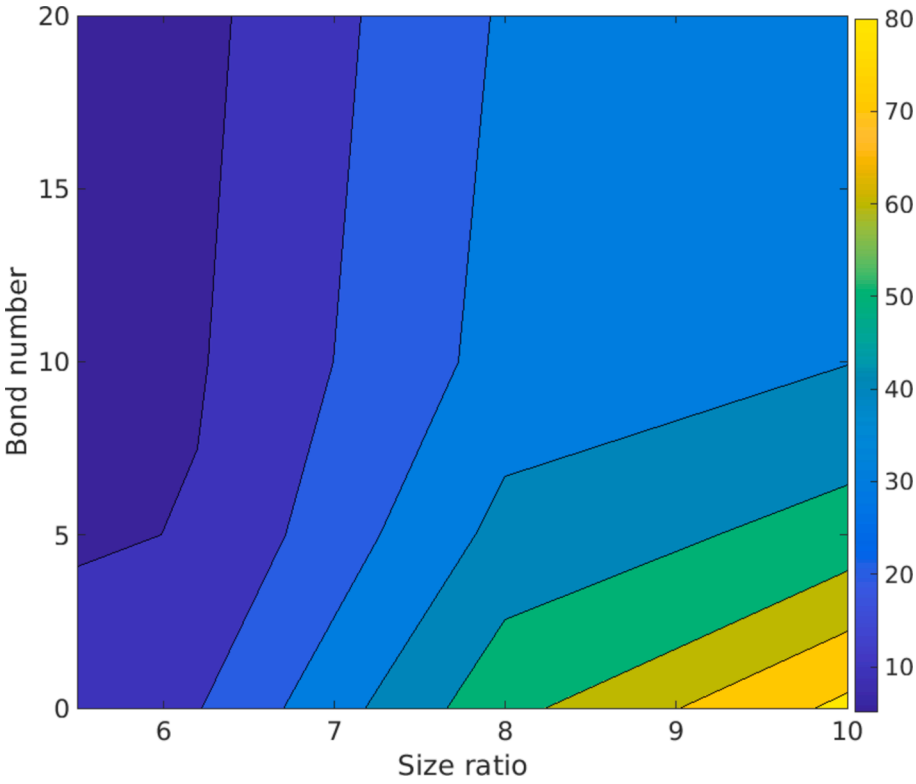

Fig. 20. Combined effects of size ratio and bond number on the migration and clogging behaviour of cohesive fines.

4.7. Effect of varying particle size ratios on clogging of cohesive fines

It is worth noting that while the primary focus of this study is on investigating the impact of cohesive fines with varying cohesion levels using both macro- and micro-scale observations, the impact of coarse–fine size ratios on clogging behaviour needs further elaboration. In response, several combinations of size ratios (e.g., 5.5, 6.2, 8.0, and 10) and Bo numbers (0, 5, 10, 20) were analysed in Fig. 20 to assess their combined influences on the infiltration ratios. It shows that when the size ratio is small, the available pore space within the granular medium

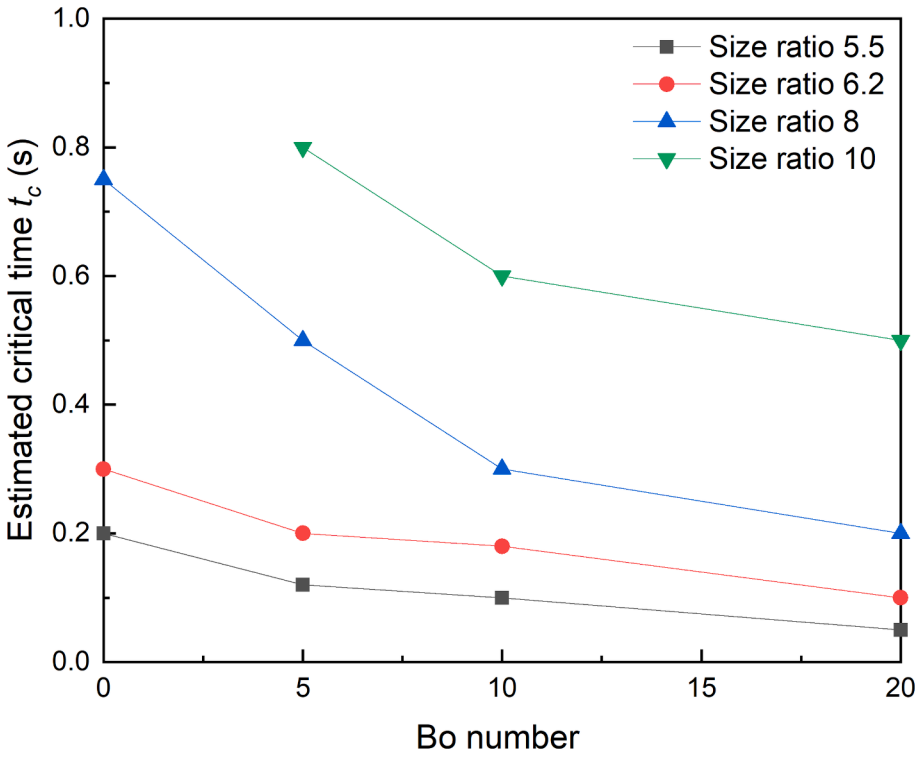

Fig. 21. Correlation of critical time with varying size ratio and Bo number.

also decreases, which subsequently increases the likelihood of clogging. For example, at a size ratio of 5.5, only 5 % of cohesive fines with Bo = 10 were able to infiltrate into the medium. In contrast, when the size ratio increases to 10, approximately 35 % of cohesive fines manages to infiltrate. This demonstrates that as the coarse-size ratio increases, the granular medium experiences a reduced risk of significant clogging, albeit still being influenced by the level of interparticle cohesion.

Moreover, the relationship between the critical time, size ratio, and Bond number (Bo) is correlated as shown in Fig. 21. The figure shows that as the size ratio increases, the critical time tends to be prolonged, delaying the onset of significant clogging. Specifically, when the size ratio reached 10 while Bo = 0 (cohesionless fines), fines continued to migrate through the coarse medium, thus no clogging occurred. This was because the pore spaces (i.e., constriction size) in the coarse medium were considerably larger than the fine particles, thus allowing continuous particle migration without significant blockage. By contrast, as the Bo number increases, the critical time sharply decreases. For instance, at a size ratio of 10, increasing the Bo number from 10 to 20 leads to about a 20 % reduction in the critical time, highlighting the prevalent role of cohesion in the clogging process. These findings underscore the importance of considering both size ratio and cohesive forces in clogging behaviour, making it crucial to integrate these factors into the development of accurate predictive models for clogging.

4.8. Micromechanical analysis of clogging

4.8.1. Variations of contact numbers with cohesion levels

The main focus of this section is to differentiate the clogging behaviour of fines with varying cohesion levels at microscale perspective, which has not been thoroughly investigated in the past. The following section presents the micromechanical analysis focused on the evolution of contact numbers between coarse and fine particles in response to fluid flow. The computation involves assessing the contact numbers among different pairs of particle types, namely coarse-coarse (C–C), fine-fine (F-F), and coarse–fine (C-F) with different levels of cohesion. The results of these contact behaviours changing with time and cohesion degree are represented in Fig. 22. It is worth noting that an inital stress condition of 20 kPa was applied vertically across the DEM region and horizontally at the fine particle region to replicate the stress distribution surrounding the granular medium. However, due to the inherent difference in stress transmission capabilities between fine and coarse particles, the fine particles reduced their capability to transmit stress effectively. This discrepancy can make the coarse particles dilate (bulging), resulting in the reduction in coarse-coarse (C–C) contacts as shown in Fig. 22a. Subsequently, increasing horizontal fluid flow drove coarse particles inwards (i.e., confinement due to hydraulic forces) and enhanced the C–C contact numbers. Moreover, the influence of cohesion levels on C–C contacts appears less significant, as indicated by the similar trend observed across all cases.

On the other hand, the interactions amongst fine particles show an interesting pattern that strongly reflects the influence of varying cohesion, as shown in Fig. 22b. Under fluid flow, initially loose fines are driven closer together so that the F-F contact number increases significantly at an earlier time (i.e., consolidation with decreasing void ratio). The cohesionless fines experience a slight decrease after the initial peak in F-F contact number, however, for cohesive particles, the F-F contacts are sustained over time with Bo $\geq$ 5. This persistence highlights the influence of interparticle cohesion in maintaining and strengthening the contacts of fine particles against the driving influence of fluid forces (resistance to internal erosion). Different from the fine-fine (F-F) contacts, Fig. 22c shows the interaction between coarse and fine particles when cohesion is considered. Expectedly, the number of coarse–fine (C-F) contacts increases when the fines migrate through the porous media regardless of the cohesion levels. Obviously, for cohesionless fines (Bo = 0), the C-F contact number escalates significantly with time as individual fines have greater freedom in moving through the relatively coarse matrix prior to any clogging. In contrast, when interparticle cohesion is considered in the case of Bo = 10, the C-F contact experiences a significant reduction of 60 % compared to the cohesionless case. This again reinforces the fact that the interaction of cohesive fines with coarse particles is marginal or insignificant as increasing cohesion limits fines migration and mobility. The variations of coarse-coarse (C–C),

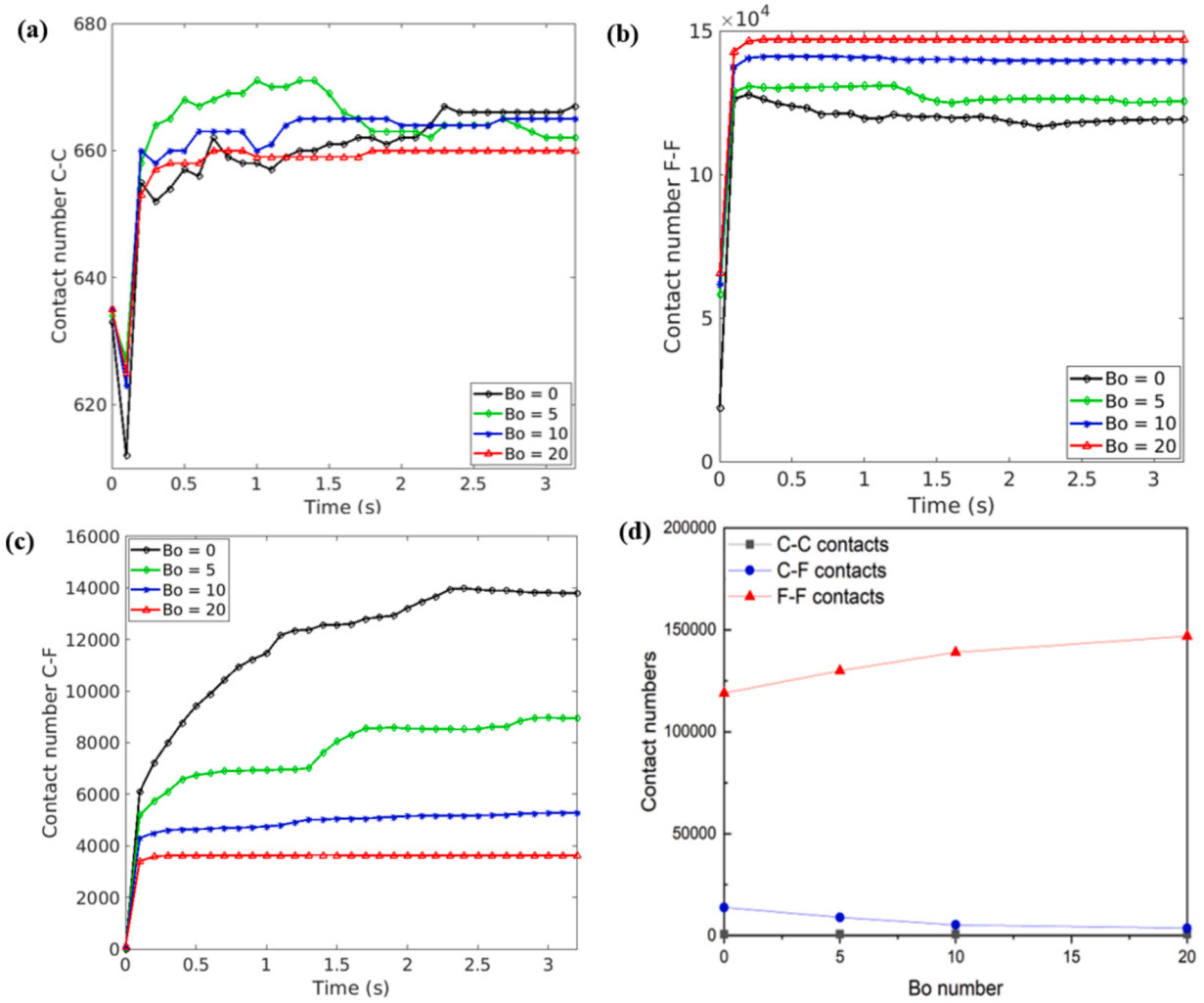

Fig. 22. Contact behaviour between fines and coarse particles for varying cohesion levels.

coarse–fine (C-F) and fine-fine (F-F) contacts with cohesion levels are summarised in Fig. 22d. This clearly shows that F-F contacts increase considerably with cohesion levels, while C-F contacts decrease. This signifies that where the cohesive force is more dominant, interparticle cohesion enhances the contacts between fine particles while limiting the migration of fines to interact with the coarse matrix.

Moreover, a detailed examination of the frequency of contact numbers by fines for two distinct cases including cohesionless (Bo = 0) and highly cohesive particles (Bo = 20) is presented in Fig. 23. The frequency represents the density distribution of contact numbers in the contact network that facilitates understanding of changes in fabric of granular media under the effect of cohesion. This analysis reveals that as the Bond number increases, there is a significant uptick in the frequency of particles which exhibit greater connectivity with their neighbours. Without the presence of cohesion, the highest frequency of contacts that fine particles experience is around 4, which is a typical value of cohesionless assemblies (Deng and Davé, 2013). As fines become more cohesive, they are more likely to form stable and interconnected networks with a greater frequency of the individual contact numbers exceeding 8 (i.e., more than 30 % increase in the frequency). These cohesive networks enhance particle retention within the medium as the increased connectivity prevents fines from being easily washed away, leading to the larger accumulation of fines and potential blockages.

4.8.2. *Variations of contact force networks (normal force) between fines with cohesion levels*

Fig. 24 displays the contact force networks when fines interact with the porous medium, represented by two representative cases for the same given coarse matrix (size ratio 8) involving cohesionless fines (Bo = 0) and cohesive fines (Bo = 20). In this presentation, it is important to note that lines connecting particles in contacts have distinct colours and thicknesses; for instance, the colour gradient changing from blue to red denotes the shift from weaker to stronger forces. The thicknesses of the lines are proportional to the magnitudes of the forces. Based on initial observation, the force network gradually develops as the quantity of fine particles passing through the granular medium gradually increases under the influence of fluid force. In the case of cohesionless fines, the contact networks between fine-fine and fine-coarse particle interactions are widely dispersed across the sample, indicating significant interactions between fines and coarse particles. By contrast, it can be intuitively observed in Fig. 24 that the cohesive fines exhibit a closely connected contact force network characterised by stronger fine-fine contacts, particularly in the surface region. This enhances the resistance against the drag force and hence limits the mobilisation of fine particles even when subjected to increasing hydraulic forces generated by fluid flow.

To quantify the differences in contact forces between cohesionless and cohesive fines, the average contact forces among fine particles were computed as shown in Fig. 25. The study further examines this trend across a wider range of Bo numbers, i.e., increasing from 0 to 5, 10, and

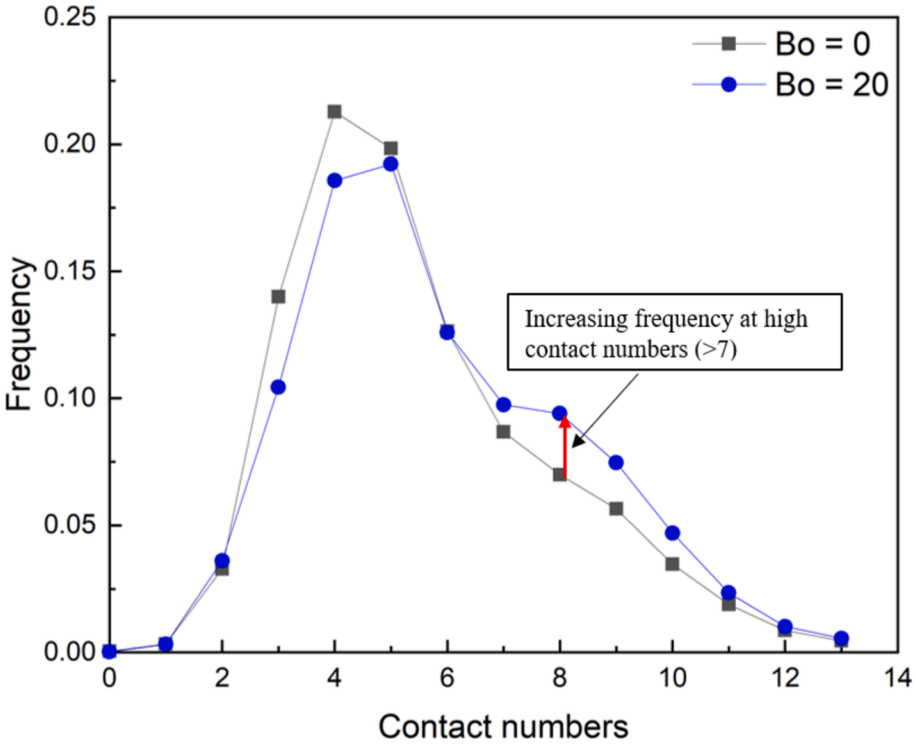

Fig. 23. Frequency of contact numbers with varying levels of cohesion

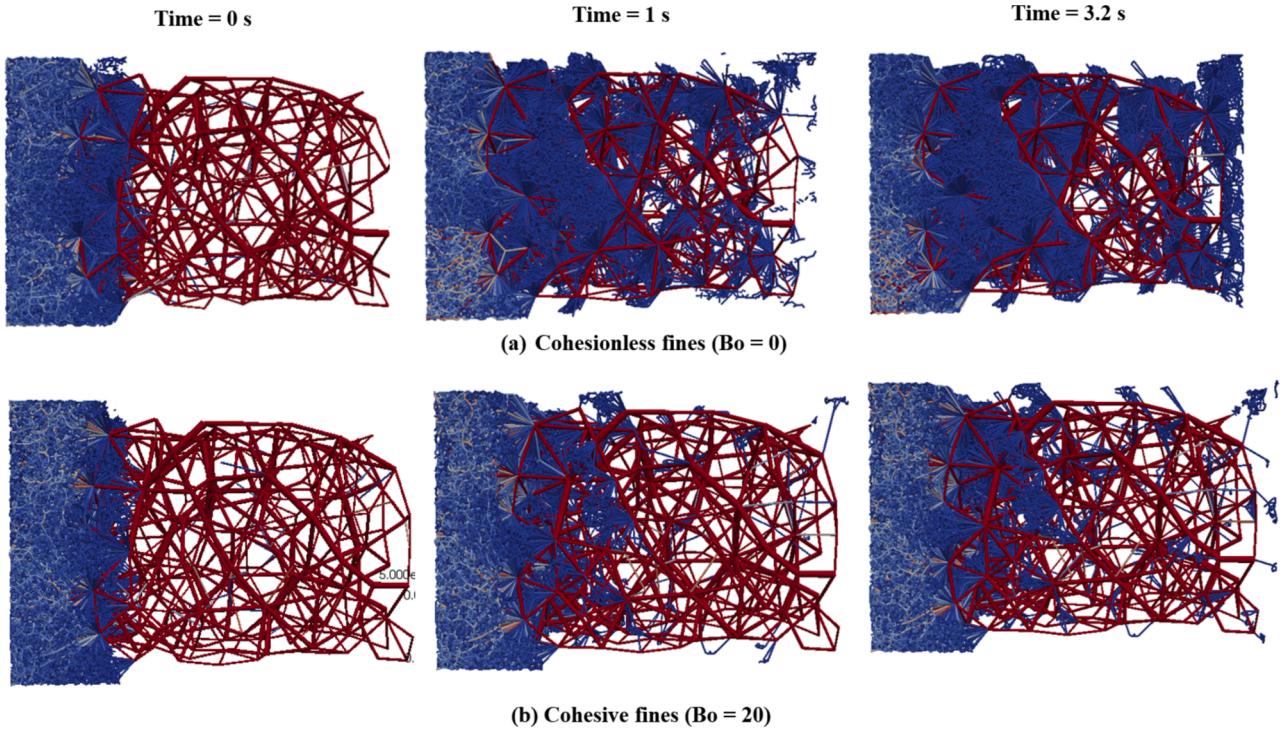

Fig. 24. Evolutions of contact force networks in the fine-coarse particle interface for two different cases: a) cohesionless and b) cohesive fines.

20. When Bo number is small (< 10), the contact force magnitude tends to fluctuate greatly and decreases with time due to ongoing disturbances from hydraulic forces. As the Bo number increases, the microscale cohesive forces significantly strengthen the contact network and leads to a more robust structure. The results reveal that the average contact force between cohesive fines is approximately 1.5 times larger than that of cohesionless particles when Bo number reaches 20. This enhanced contact network correlates positively with the material's increased shear and cohesive strength. The higher cohesion-induced strength enables the cohesive fines to exhibit greater resistance against fluid-driven forces, which promotes particle deposition and exacerbates the clogging process.

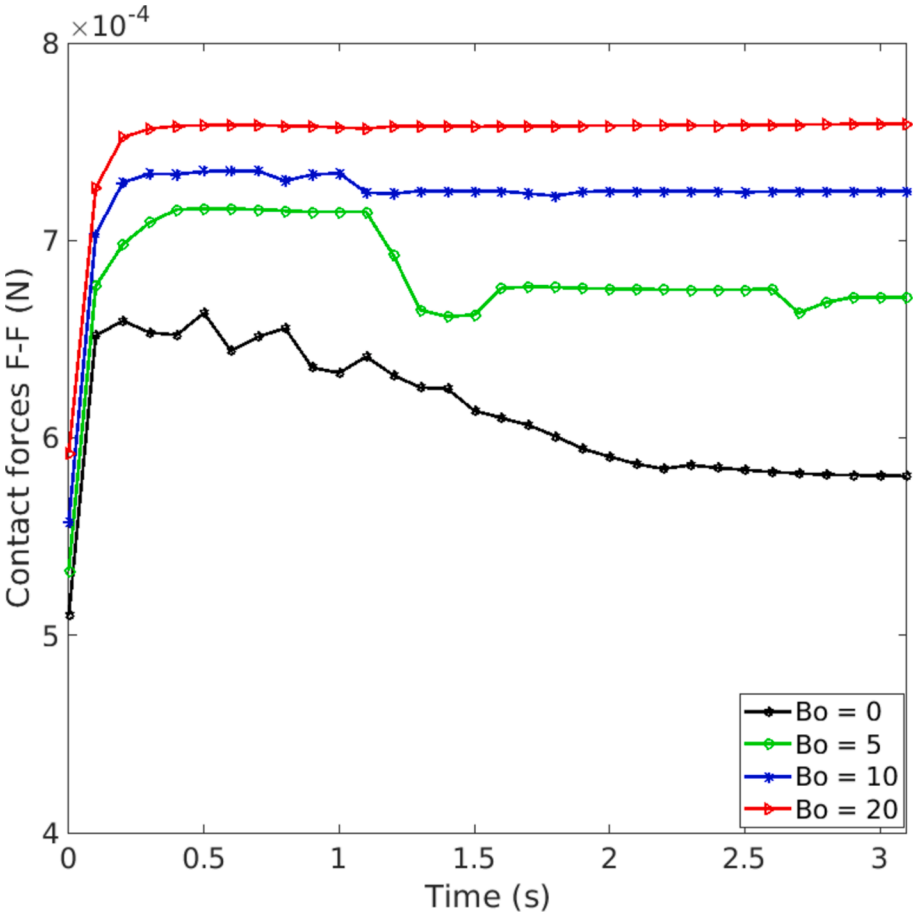

Fig. 25. Quantification of contact forces amongst fine particles with a wide range of Bo numbers.

4.8.3. Influence of cohesion-induced agglomeration on clogging process

The preceding sections have shown that cohesive fines exhibit a greater potential to induce particle deposition and clogging compared to their cohesionless counterparts. This is attributed to the tendency of cohesive particles to coalesce into larger agglomerates under the influence of strong cohesive interactions. This phenomenon, termed cohesion-induced agglomeration, plays a significant role in elucidating the clogging behaviour of cohesive materials. Specifically, as the interparticle cohesion dominates, the agglomeration effect becomes more prominent (Afrassiabian et al., 2020). Although previous studies (Deng et al., 2018; Seville et al., 2000) have intuitively correlated the agglomeration effect with cohesive fines, they focused different contexts that lack relevant considerations of soil clogging, especially at the interface of fine-granular column. More importantly, the generation and stabilisation of agglomerations induced by varying cohesion are complex process that none of past studies could quantify. Innovatively, the current study quantitatively examines the formation of agglomerates of cohesive soil with different degrees of cohesion and uses them to further elucidate clogging process under horizontal seepage flow. The evaluation of agglomerate formation follows three criteria:

(i) contacting particles are detected when the interparticle distance between two particles is smaller than their combined sizes,
(ii) the minimum contacting duration persists more than 0.1 s to distinguish between stable and unstable clusters, and
(iii) agglomerates are counted only if they consist of at least five particles.

A flowchart representing the procedure to detect and characterise particle contacts and agglomerates proposed and used in the current study is presented in Fig. 26.

Furthermore, the influence of interparticle cohesion on the formation and stability of agglomerates is investigated in Fig. 27. It shows that when interparticle cohesion is small (< 10), the number of agglomerates fluctuates significantly over time, indicating the temporary nature of agglomeration formation and breakage. This implies that while cohesionless particles may collide and briefly form clusters, these structures are unstable and easily disrupted due to the lack of interparticle bonding. In contrast, with highly cohesive fines (Bo > 10), a greater number of stable agglomerates are formed that persist over longer periods. These findings elucidate the role of cohesion in maintaining stable agglomerates, which is consistent with previous studies on the behaviour of micro-sized iron fines in fluidisation simulations (Liu et al., 2023). However, unlike Liu et al. (2023), the current research focuses on clogging interactions between fines and coarse granular media under influences of various factors such as cohesion, fluid flow (rising hydraulic gradient) and confining pressure.

Further visualisations of the dynamic formation and disintegration processes of agglomerates over time under varying cohesion and fluid flow are presented in Fig. 28. It shows that cohesionless particles (Bo $=$ 0) form initial contacts in Fig. 28a, however, these interactions are easily disintegrated under increasing hydraulic forces. For instance, as the hydraulic gradient increases with time (i.e., Fig. 28b, time $= 1$ s), these particles are observed to flow as individuals rather than remaining in agglomerated forms. In contrast, when cohesive forces come into play (Bo $= 20$) as shown in Fig. 28c and Fig. 28d, fine particles leverage cohesive interactions to form agglomerates (i.e., CN > 5) that remain stable against the increasing hydraulic gradient over time.

Following the visual detection of agglomerate formation in Fig. 28, this section presents a detailed elaboration on why the increased size of

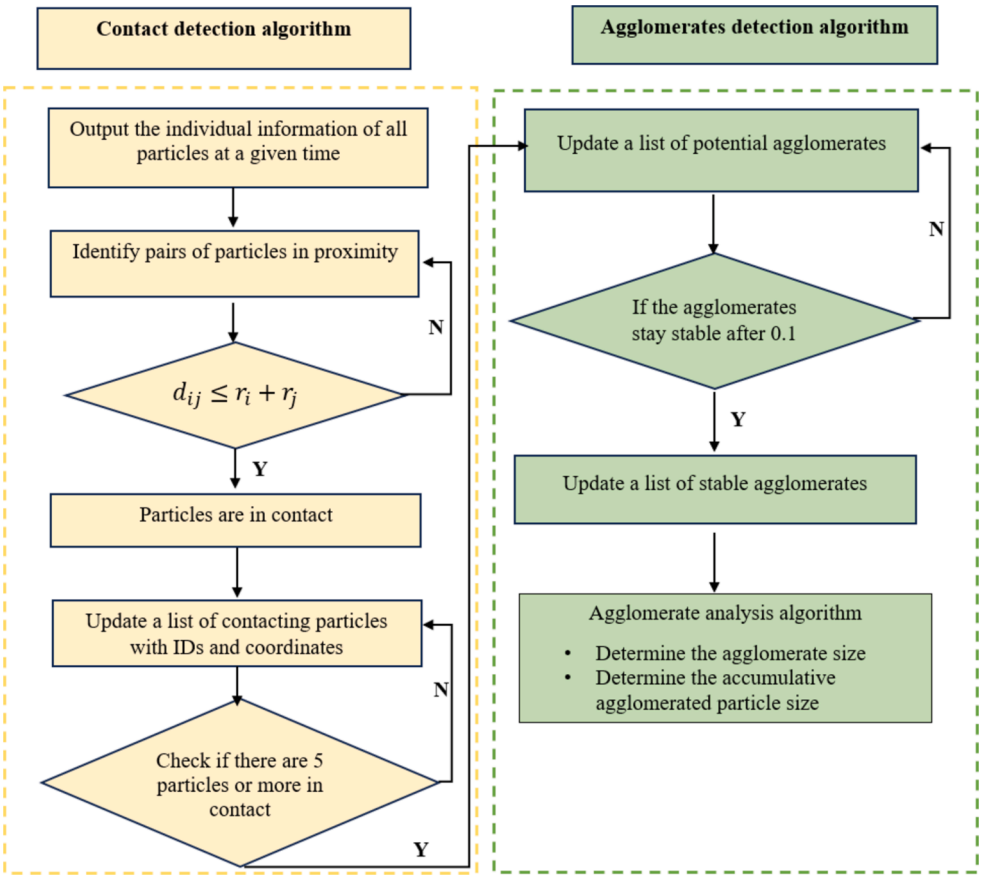

Fig. 26. Algorithm to determine and characterise stable agglomerates in the current numerical simulations.

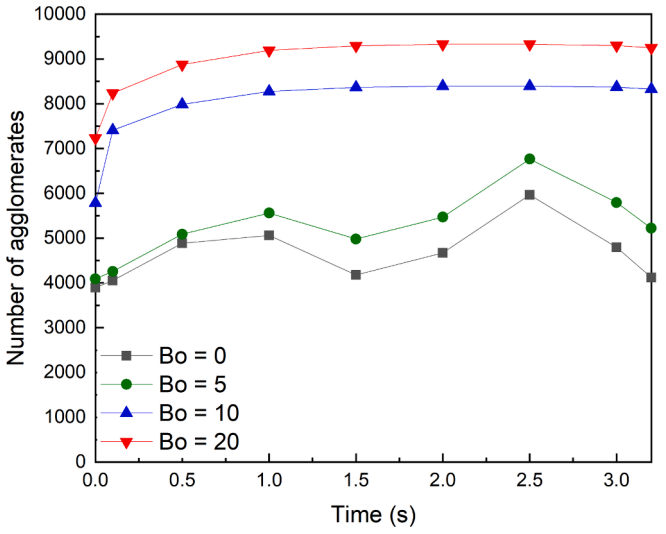

Fig. 27. The evolution of agglomerates over time considering different degrees of cohesion via Bo numbers.

agglomerates should be taken into account when investigating the clogging mechanisms in porous systems. Fig. 29 quantifies the cumulative size distribution of agglomerated particles at the end of the simulation, particularly in the scenario where particle cohesion is pronounced. This comparison against the original PSD of fines reveals significant alterations due to agglomeration. This process not only widens the range of particle sizes within the system but also induces a notable shift in the median particle size towards larger sizes. This shift in PSD caused by the presence of cohesion has been experimentally observed in previous experimental studies (Zhang et al., 2023), however, there was a lack of quantitative characterisation as being addressed in the current study. In the context of clogging, as these agglomerates behave as larger effective size particles, they can surpass the critical constriction size of coarse matrix and contribute to the clogging potential. Moreover, they offer increased resistance to the fluid flow, facilitating particle deposition within the porous medium and increasing the likelihood of clogging. This understanding is particularly crucial in the design and operational phases of filtration and drainage systems whereas existing design criteria (Indraratna et al., 2007; Israr and Indraratna, 2017; Terzaghi, 1926) based on uniform or narrowly distributed PSDs of cohesionless fines may no longer suffice. Instead, design models need to incorporate the potential for significant PSD widening and the formation of large agglomerates under certain conditions. This includes considering the effects of varying cohesion levels such as the Bond number on the PSD and the consequent clogging behaviour.

5. Conclusions

This study adopted a combined CFD-DEM approach to explore the dynamics of fine particles migrating and clogging within the granular medium under rising hydraulic flow and interparticle cohesion. On the one hand, the macroscopic behaviour of particle migration and clogging was assessed through metrics such as the infiltration ratio, and the spatial distribution of infiltrated particles, and the deposition coefficient. On the other hand, the micro-mechanisms of these phenomena were also examined, including the detailed evolution in contact behaviour between fines and coarse particles, and the contact force networks. More importantly, a novel aspect of this investigation focused on the quantitative analysis of agglomeration induced by the

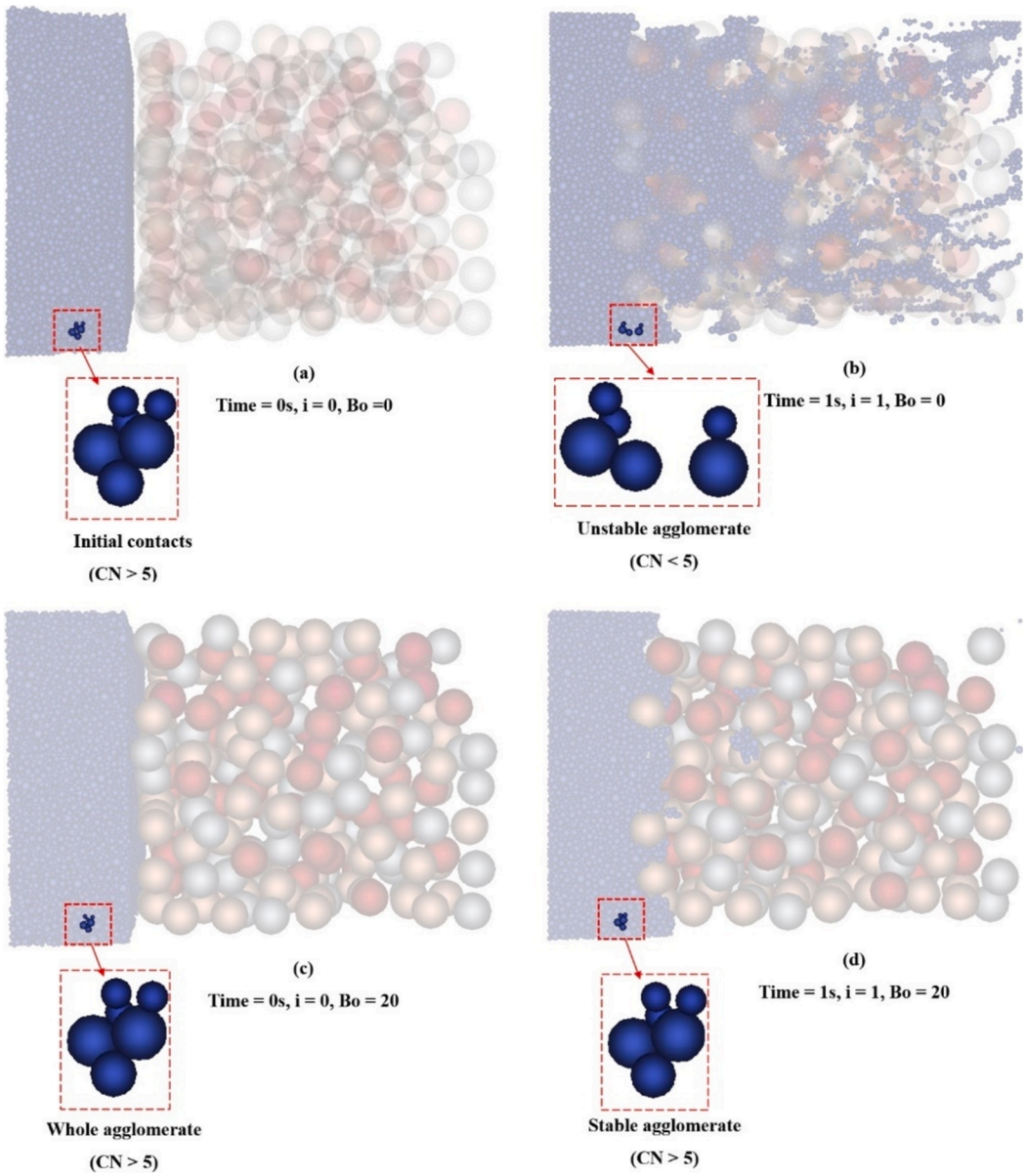

Fig. 28. The evolution of representative agglomerate with time under rising hydraulic flow in (a-b) cohesionless fines and (c-d) cohesive fines (Bo = 20).

interparticle attractive forces, elucidating the process of agglomerate formation and stability under varying levels of cohesion. The salient findings from this study are summarised as follows:

- For cohesionless fines, when the size ratio was relatively low (i.e., < 8), the infiltration of particles modestly increased to around 19 % and stabilised early despite increasing hydraulic gradients. However, in the cases of larger size ratios (i.e., 8 and 10), the infiltration of fines showed a continuous increase with an ultimate accumulation of over 50 % to 80 % fine particles retained in the granular medium respectively.
- The presence of interparticle cohesion via Bo numbers was found to profoundly affect particle migration and clogging phenomenon. For instance, for the size ratio = 8, the infiltration ratio was halted from 57 % to 31 % when Bo numbers increased from 0 to 20. Moreover, by monitoring the ongoing movements of fine particles into the coarse medium with time, the entire infiltration process can be categorised into three distinct phases: initial infiltration, steady increase and stabilisation. As cohesion increased, the infiltration changed from a non-smooth and *meta*-stabilisation to an immediate stabilisation that occurred at early stage.
- More importantly, the numerical outcomes embraced a novel contribution in regard to estimating the rate and extent of the clogging process by determining the unclogged radius and the critical time, which was missing in the past literature. The results yielded the critical time at around 30 % of the total time needed to reach substantial clogging. In this condition, the clogged radius occupied almost 20 % of the outer periphery of the column, and the permeability of the clogged granular medium decreased to about 50 % of its original value with obvious implications on drainage. Moreover, a wide range of critical time was computed for varying size ratios and cohesion level, which highlighted the importance role of considering both size ratio and cohesive forces in clogging investigation.
- The results from micromechanical analysis led to a conclusion that the presence of interparticle cohesion resulted in a notable increase in fine-fine contacts (20 % increase), while coarse–fine (C-F) contacts decreased by approximately 60 % compared to the cohesionless counterpart. This suggested that dominant cohesive forces enhanced

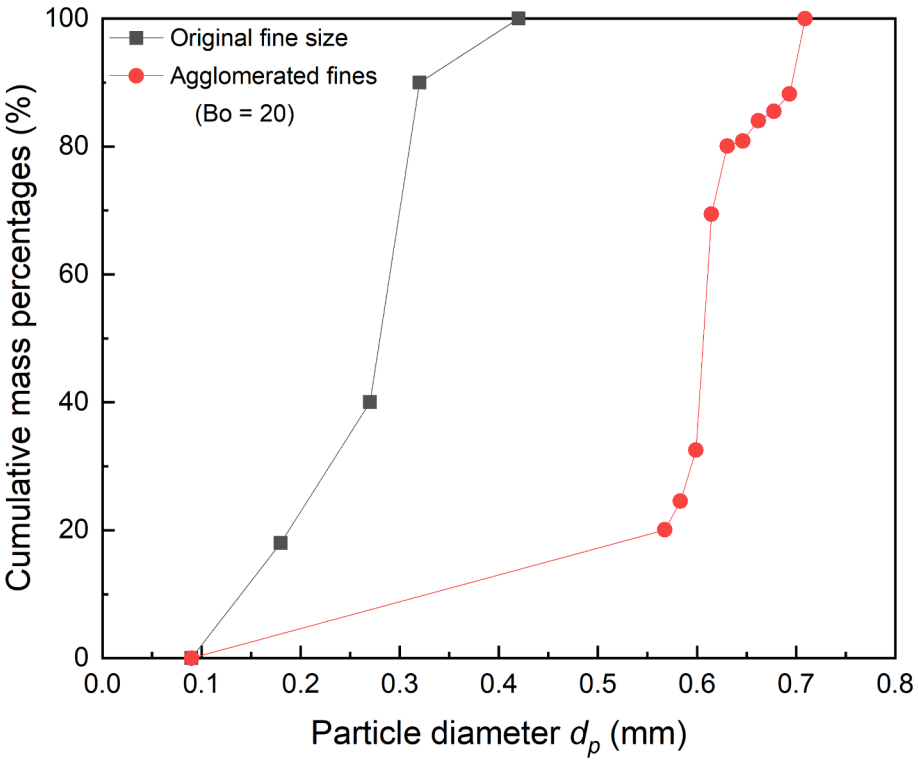

Fig. 29. Changes in PSD of fines with agglomeration caused by interparticle cohesion

connectivity among fine particles while restricting their interactions with the coarse matrix.

- The clogging mechanism of cohesive fines can be attributed to their propensity to coalesce into larger and stable agglomerates with increasing cohesion. It was observed that cohesive fine particles leveraged the interparticle bonds to form and stabilise a significantly higher number of agglomerates (> 9000) compared to the cohesionless case where the agglomerate numbers greatly fluctuated. In the context of clogging, these agglomerates behaved as larger effective size particles, which can surpass the critical constriction size of the coarse matrix and contribute an increased potential for clogging. Moreover, clusters of particles exhibited a greater resistance against the flow of fluid, hence promoting the retention and deposition of particles within the porous medium and further exacerbating the clogging issue.

CRediT authorship contribution statement

Thao Doan: Writing – review & editing, Writing – original draft, Validation, Methodology, Investigation, Formal analysis, Data curation, Conceptualization. **Buddhima Indraratna:** Writing – review & editing, Supervision, Project administration, Methodology, Investigation, Funding acquisition, Conceptualization. **Thanh T. Nguyen:** Writing – review & editing, Supervision, Methodology, Investigation. **Cholachat Rujikiatkamjorn:** Writing – review & editing, Supervision, Investigation.

Declaration of competing interest

The authors declare that they have no known competing financial interests or personal relationships that could have appeared to influence the work reported in this paper.

Acknowledgements

This research was supported by Transport Research Centre (TRC, UTS), and the Australian Government through the Australian Research Council's funding scheme (project LP160101254 **and** DE230101127). Technical and financial support from industry partners including SMEC, Sydney Trains, ACRI and Coffey are greatly appreciated

Data availability

Data will be made available on request.

References

Afrassiabian, Z., Leclerc, W., Guessasma, M., Saleh, K., 2020. Numerical simulation of mechanical resistance of wet and dry powder cakes. Powder Technol. 371, 45–54. https://www.sciencedirect.com/science/article/pii/S0032591020304034.

Ajmal, M., Roessler, T., Richter, C., Katterfeld, A., 2020. Calibration of cohesive DEM parameters under rapid flow conditions and low consolidation stresses. Powder Technol. 374, 22–32. https://www.sciencedirect.com/science/article/pii/S003259102030632X.

Alem, A., Elkawafi, A., Ahfir, N.-D., Wang, H., 2013. Filtration of kaolinite particles in a saturated porous medium: Hydrodynamic effects. Hydrgeol. J. 21 (3), 573–586. https://doi.org/10.1007/s10040-012-0948-x.

Anderson, J.D., Wendt, J., 1995. Computational fluid dynamics. Springer.

Barthel, E., 2008. Adhesive elastic contacts: JKR and more. J. Phys. D Appl. Phys. 41 (16), 163001.

Basack, S., Siahaan, F., Indraratna, B., Rujikiatkamjorn, C., 2018. Stone column-stabilized soft-soil performance influenced by clogging and lateral deformation: Laboratory and numerical evaluation. Int. J. Geomech. 18 (6), 04018058. https://doi.org/10.1061/(ASCE)GM.1943-5622.0001148.

Bennacer, L., Ahfir, N.-D., Alem, A., Huaqing, W., 2022. Influence of particles sizes and flow velocity on the transport of polydisperse fine particles in saturated porous media: Laboratory experiments. Water Air Soil Pollut. 233 (7), 249. https://doi.org/10.1007/s11270-022-05732-4.

Black, J.A., Sivakumar, V., Bell, A., 2011. The settlement performance of stone column foundations. Géotechnique 61 (11), 909–922. https://www.icevirtuallibrary.com/doi/abs/10.1680/geot.9.P.014.

Carman, P.C., 1937. Fluid flow through a granular bed. Trans. Inst. Chem. Eng. London 15, 150–156.

Castellanos, A., 2005. The relationship between attractive interparticle forces and bulk behaviour in dry and uncharged fine powders. Adv. Phys. 54 (4), 263–376. https://doi.org/10.1080/17461390500402657.

Chen, X.-X., Cai, Q.-P., Wu, Z.-H., 2017. Experimental and theoretical study of coupled influence of flow velocity increment and particle size on particle retention and

release in porous media. Water Sci. Eng. 10 (3), 236–245. https://www.sciencedirect.com/science/article/pii/S1674237017300820.
Coetzee, C. J. (2020). *Simplified Johnson-Kendall-Roberts (SJKR) Contact Model - Implementation in PFC*.
Deng, X.L., Davé, R.N., 2013. Dynamic simulation of particle packing influenced by size, aspect ratio and surface energy. Granul. Matter 15 (4), 401–415. https://doi.org/10.1007/s10035-013-0413-0.
Deng, Y., Liu, L., Cui, Y.-J., Feng, Q., Chen, X., He, N., 2018. Colloid effect on clogging mechanism of hydraulic reclamation mud improved by vacuum preloading. Can. Geotech. J. 56 (5), 611–620. https://doi.org/10.1139/cgj-2017-0635.
Derakhshani, S.M., Schott, D.L., Lodewijks, G., 2015. Micro–macro properties of quartz sand: Experimental investigation and DEM simulation. Powder Technol. 269, 127–138. https://www.sciencedirect.com/science/article/pii/S0032591014007888.
Derjaguin, B.V., Muller, V.M., Toporov, Y.P., 1975. Effect of contact deformations on the adhesion of particles. J. Colloid Interface Sci. 53 (2), 314–326. https://www.sciencedirect.com/science/article/pii/0021979775900181.
Di Felice, R., 1994. The voidage function for fluid-particle interaction systems. Int. J. Multiph. Flow 20 (1), 153–159. https://www.sciencedirect.com/science/article/pii/0301932294900116.
Doan, T., Indraratna, B., Nguyen, T.T., Rujikiatkamjorn, C., 2023. Interactive Role of Rolling Friction and Cohesion on the Angle of Repose through a Microscale Assessment. Int. J. Geomech. 23 (1), 04022250. https://doi.org/10.1061/(ASCE)GM.1943-5622.0002632.
El Shamy, U., Zeghal, M., 2005. Coupled continuum-discrete model for saturated granular soils. J. Eng. Mech. 131 (4), 413–426. https://doi.org/10.1061/(ASCE)0733-9399(2005)131:4(413).
Elrahmani, A., Al-Raoush, R.I., Seers, T.D., 2023. Clogging and permeability reduction dynamics in porous media: A numerical simulation study. Powder Technol. 427, 118736. https://www.sciencedirect.com/science/article/pii/S003259102300520X.
Erdim, E., Akgiray, Ö., Demir, İ., 2015. A revisit of pressure drop-flow rate correlations for packed beds of spheres. Powder Technol. 283, 488–504. https://www.sciencedirect.com/science/article/pii/S0032591015004726.
Foster, M., Fell, R., 2001. Assessing embankment dam filters that do not satisfy design criteria. J. Geotech. Geoenviron. Eng. 127 (5), 398–407. https://doi.org/10.1061/(ASCE)1090-0241(2001)127:5(398).
Gibson, S., Abraham, D., Heath, R., Schoellhamer, D., 2010. Bridging process threshold for sediment infiltrating into a coarse substrate. J. Geotech. Geoenviron. Eng. 136 (2), 402–406. https://doi.org/10.1061/(ASCE)GT.1943-5606.0000219.
Grima, A. P. (2011). "Quantifying and modelling mechanisms of flow in cohesionless and cohesive granular materials.".
Hu, Z., Zhang, Y., Yang, Z., 2019. Suffusion-induced deformation and microstructural change of granular soils: A coupled CFD–DEM study. Acta Geotech. 14 (3), 795–814. https://doi.org/10.1007/s11440-019-00789-8.
Indraratna, B., Raut Ashok, K., Khabbaz, H., 2007. Constriction-based retention criterion for granular filter design. J. Geotech. Geoenviron. Eng. 133 (3), 266–276. https://doi.org/10.1061/(ASCE)1090-0241(2007)133:3(266).
Indraratna, B., Basack, S., Rujikiatkamjorn, C., 2013. Numerical solution of stone column-improved soft soil considering arching, clogging, and smear effects. J. Geotech. Geoenviron. Eng. 139 (3), 377–394. https://doi.org/10.1061/(ASCE)GT.1943-5606.0000789.
Indraratna, B., Phan Nghi, M., Nguyen Thanh, T., Huang, J., 2021. Simulating subgrade soil fluidization using LBM-DEM coupling. Int. J. Geomech. 21 (5), 04021039. https://doi.org/10.1061/(ASCE)GM.1943-5622.0001997.
Israr, J., Indraratna, B., 2017. Internal stability of granular filters under static and cyclic loading. J. Geotech. Geoenviron. Eng. 143 (6), 04017012. https://doi.org/10.1061/(ASCE)GT.1943-5606.0001661.
Jiang, M.J., Konrad, J.M., Leroueil, S., 2003. An efficient technique for generating homogeneous specimens for DEM studies. Comput. Geotech. 30 (7), 579–597. https://www.sciencedirect.com/science/article/pii/S0266352X03000648.
Johnson, K. L., Kendall, K., Roberts, A. D., and Tabor, D. (1971). "Surface energy and the contact of elastic solids." *Proceedings of the Royal Society of London. A. Mathematical and Physical Sciences*, 324(1558): 301-313. Doi: 10.1098/rspa.1971.0141.
Jones, R., 2003. From single particle AFM studies of adhesion and friction to bulk flow: Forging the links. Granul. Matter 4 (4), 191–204. https://doi.org/10.1007/s10035-002-0122-6.
Kafui, K.D., Thornton, C., Adams, M.J., 2002. Discrete particle-continuum fluid modelling of gas–solid fluidised beds. Chem. Eng. Sci. 57 (13), 2395–2410. https://www.sciencedirect.com/science/article/pii/S0009250902001409.
Kanitz, M., Grabe, J., 2021. The influence of the void fraction on the particle migration: A coupled computational fluid dynamics–discrete element method study about drag force correlations. Int. J. Numer. Anal. Meth. Geomech. 45 (1), 45–63. https://doi.org/10.1002/nag.3131.
Kim, Y.S., Whittle, A.J., 2006. Filtration in a porous granular medium: 1. Simulation of pore-scale particle deposition and clogging. Transp. Porous Media 65 (1), 53–87. https://doi.org/10.1007/s11242-005-6087-2.
Kloss, C., Goniva, C., König, A., Amberger, S., Pirker, S., 2012. Models, algorithms and validation for opensource DEM and CFD-DEM. Prog. Comput. Fluid Dyn. 12, 140–152.
Lin, Y., Fang, Y., He, C., 2022. Numerical study on clogging mechanism of slurry infiltration in porous media based on coupled CFD-DEM method. Tunn. Undergr. Space Technol. 128, 104622. https://www.sciencedirect.com/science/article/pii/S0886779822002620.
Lippera, M.C., Werban, U., Vienken, T., 2023. Improving clogging predictions at managed aquifer recharge sites: A quantitative assessment on the vertical distribution of intrusive fines. Hydrgeol. J. 31 (1), 71–86. https://doi.org/10.1007/s10040-022-02581-7.
Liu, X., Hessels, C.J.M., Deen, N.G., Tang, Y., 2023. CFD-DEM investigation on the agglomeration behavior of micron-sized combusted iron fines. Fuel 346, 128219. https://www.sciencedirect.com/science/article/pii/S0016236123008323.
Liu, P., Sun, M., Chen, Z., Zhang, S., Zhang, F.-S., Chen, Y., Chen, W., Bate, B., 2023. Influencing factors on fines deposition in porous media by CFD–DEM simulation. Acta Geotech. 18 (9), 4539–4563. https://doi.org/10.1007/s11440-023-01870-z.
Liu, Y., Yin, Z.-Y., Wang, L., Hong, Y., 2020. A coupled CFD–DEM investigation of internal erosion considering suspension flow. Can. Geotech. J. 58 (9), 1411–1425. https://doi.org/10.1139/cgj-2020-0099.
Locke, M., Indraratna, B., Adikari, G., 2001. Time-dependent particle transport through granular filters. J. Geotech. Geoenviron. Eng. 127 (6), 521–529. https://doi.org/10.1061/(ASCE)1090-0241(2001)127:6(521).
Lommen, S., Schott, D., Lodewijks, G., 2014. DEM speedup: Stiffness effects on behavior of bulk material. Particuology 12, 107–112. https://www.sciencedirect.com/science/article/pii/S1674200113001387.
Mesticou, Z., Kacem, M., and Dubujet, P. (2016). "Coupling Effects of Flow Velocity and Ionic Strength on the Clogging of a Saturated Porous Medium." *Transport in porous Media. (DOI 10.1007/s11242-016-0644-8)*, 112.
Nguyen, T., Indraratna, B., 2019. Micro-CT scanning to examine soil clogging behavior of natural fiber drains. J. Geotech. Geoenviron. Eng. 145, 04019037.
Nguyen, T.T., Indraratna, B., 2020. A coupled CFD–DEM approach to examine the hydraulic critical state of soil under increasing hydraulic gradient. Int. J. Geomech. 20 (9), 04020138. https://doi.org/10.1061/(ASCE)GM.1943-5622.0001782.
Nguyen, T.T., Indraratna, B., 2022. Fluidization of soil under increasing seepage flow: An energy perspective through CFD-DEM coupling. Granul. Matter 24 (3), 80. https://doi.org/10.1007/s10035-022-01242-6.
Nguyen, T.T., Indraratna, B., 2022. Rail track degradation under mud pumping evaluated through site and laboratory investigations. Int. J. Rail Transp. 10 (1), 44–71. https://doi.org/10.1080/23248378.2021.1878947.
O'Sullivan, C., 2011. Particulate discrete element modelling a geomechanics perspective. Taylor & Francis, London.
Pal, S., Deb, K., 2019. Effect of clogging of stone column on drainage capacity during soil liquefaction. Soils Found. 59 (1), 196–207. https://www.sciencedirect.com/science/article/pii/S0038080618302105.
Parteli, E.J.R., Schmidt, J., Blümel, C., Wirth, K.-E., Peukert, W., Pöschel, T., 2014. Attractive particle interaction forces and packing density of fine glass powders. Sci. Rep. 4 (1), 6227. https://doi.org/10.1038/srep06227.
Parvan, A., Jafari, S., Rahnama, M., Norouzi apourvari, S., and Raoof, A. (2020). "Insight into particle retention and clogging in porous media; a pore scale study using lattice Boltzmann method." *Advances in Water Resources*, 138: 103530. https://www.sciencedirect.com/science/article/pii/S0309170819310401.
Phan, Q.T., Bui, H.H., Nguyen, G.D., Bouazza, A., 2021. Effect of particle rolling resistance on drained and undrained behaviour of silty sand. Acta Geotech. 16 (8), 2657–2682. https://doi.org/10.1007/s11440-020-01128-y.
Prempeh, K.O.K., Chequer, L., Badalyan, A., Bedrikovetsky, P., 2020. Effects of the capillary-entrapped phase on fines migration in porous media. J. Nat. Gas Sci. Eng. 73, 103047. https://www.sciencedirect.com/science/article/pii/S1875510019302999.
Rao, Y., Fu, H., Yang, T., Chen, H., Zhang, Z., Ding, H., 2022. Comparison between sand and clay clogging mechanisms of pervious concrete pavement. Sci. Rep. 12 (1), 9258. https://doi.org/10.1038/s41598-022-13483-9.
Reddi, L.N., Bonala, M.V.S., 1997. Analytical solution for fine particle accumulation in soil filters. J. Geotech. Geoenviron. Eng. 123 (12), 1143–1152. https://doi.org/10.1061/(ASCE)1090-0241(1997)123:12(1143).
Seville, J.P.K., Willett, C.D., Knight, P.C., 2000. Interparticle forces in fluidisation: A review. Powder Technol. 113 (3), 261–268. https://www.sciencedirect.com/science/article/pii/S0032591000003090.
Shi, L., Wang, Q.-Q., Xu, S.-L., Pan, X.-D., Sun, H.-L., Cai, Y.-Q., 2018. Numerical study on clogging of prefabricated vertical drain in slurry under vacuum loading. Granul. Matter 20 (4), 74. https://doi.org/10.1007/s10035-018-0846-6.
Shi, L., Jiang, J., Wang, Q., Sun, H., Yuan, Z., Pan, X., 2021. Numerical study on movements of soil particles forming clogging layer during vacuum preloading of dredged slurry. Granul. Matter 23 (4), 92. https://doi.org/10.1007/s10035-021-01151-0.
Silva, I.N., Indraratna, B., Nguyen, T.T., Rujikiatkamjorn, C., 2023. The influence of soil fabric on the monotonic and cyclic shear behaviour of consolidated and compacted specimens. Can. Geotech. J. https://doi.org/10.1139/cgj-2023-0141.
Singh, A., Magnanimo, V., Saitoh, K., Luding, S., 2014. Effect of cohesion on shear banding in quasistatic granular materials. Phys. Rev. E 90 (2), 022202. https://link.aps.org/doi/10.1103/PhysRevE.90.022202.
Tai, P., Indraratna, B., Rujikiatkamjorn, C., 2017. Experimental simulation and mathematical modelling of clogging in stone column. Can. Geotech. J. 55 (3), 427–436. https://doi.org/10.1139/cgj-2017-0271.
Tang, Y., Yao, X., Chen, Y., Zhou, Y., Zhu, D.Z., Zhang, Y., Zhang, T., Peng, Y., 2020. Experiment research on physical clogging mechanism in the porous media and its impact on permeability. Granul. Matter 22 (2), 37. https://doi.org/10.1007/s10035-020-1001-8.
Tao, J., Tao, H., 2017. Factors affecting piping erosion resistance: Revisited with a numerical modeling approach. Int. J. Geomech. 17 (11), 04017097. https://doi.org/10.1061/(ASCE)GM.1943-5622.0000999.
Tennakoon, N., Indraratna, B., Rujikiatkamjorn, C., 2014. Effect of ballast contamination on the behaviour of track substructure. Aust. Geomech. J. 49, 113–123.
Terzaghi, K. (1926). "Soil physical basis of mechanics of earth structures. F." Deuticke, Wien.

Tsuji, Y., Tanaka, T., Ishida, T., 1992. Lagrangian numerical simulation of plug flow of cohesionless particles in a horizontal pipe. Powder Technol. 71 (3), 239–250. https://www.sciencedirect.com/science/article/pii/003259109288030L.

Tsuji, Y., Kawaguchi, T., Tanaka, T., 1993. Discrete particle simulation of two-dimensional fluidized bed. Powder Technol. 77 (1), 79–87. https://www.sciencedirect.com/science/article/pii/0032591093850107.

Tsunazawa, Y., Fujihashi, D., Fukui, S., Sakai, M., Tokoro, C., 2016. Contact force model including the liquid-bridge force for wet-particle simulation using the discrete element method. Adv. Powder Technol. 27 (2), 652–660. https://www.sciencedirect.com/science/article/pii/S0921883116000698.

Ucgul, M., Fielke, J.M., Saunders, C., 2014. Three-dimensional discrete element modelling of tillage: Determination of a suitable contact model and parameters for a cohesionless soil. Biosyst. Eng. 121, 105–117. https://www.sciencedirect.com/science/article/pii/S1537511014000208.

Vowinckel, B., Withers, J., Luzzatto-Fegiz, P., Meiburg, E., 2019. Settling of cohesive sediment: Particle-resolved simulations. J. Fluid Mech. 858, 5–44. https://www.cambridge.org/core/product/3656551A753663B0F047EFF5D73E9A62.

Xie, Z., Wang, S., Shen, Y., 2023. Roles of clusters in the migration of fines through porous media. Chem. Eng. Sci. 265, 118217. https://www.sciencedirect.com/science/article/pii/S0009250922008016.

Xiong, H., Zhang, Z., Sun, X., Yin, Z.-Y., Chen, X., 2022. Clogging effect of fines in seepage erosion by using CFD–DEM. Comput. Geotech. 152, 105013. https://www.sciencedirect.com/science/article/pii/S0266352X22003500.

Xu, L., Nong, S., Dong, Y., Sun, Z., 2024. Particle-size control on the structure and collapsibility of sediments formed by air-fall deposition. Catena 236, 107743. https://www.sciencedirect.com/science/article/pii/S0341816223008342.

Xu, S., Zhu, Y., Cao, H., Sun, H., Cai, Y., Wu, J., 2022. Studying the soil column formation in soft soil improved by vacuum preloading via coupled scale-up CFD-DEM simulations. Int. J. Numer. Anal. Meth. Geomech. 46 (7), 1272–1291. https://doi.org/10.1002/nag.3345.

Yin, T., Zhang, Z., Huang, X., Shire, T., Hanley, K.J., 2021. On the morphology and pressure-filtration characteristics of filter cake formation: Insight from coupled CFD–DEM simulations. Tunn. Undergr. Space Technol. 111, 103856. https://www.sciencedirect.com/science/article/pii/S088677982100047X.

Zhang, Y., Sufian, A., and Scheuermann, A. (2023). "Influence of hydraulic and geometric conditions on the early stages of the filtration process in idealised granular soils comprising spherical particles." *International Journal for Numerical and Analytical Methods in Geomechanics*, n/a(n/a): Doi: 10.1002/nag.3583.

Zhang, R., Yang, Z., Detwiler, R., Li, D., Ma, G., Hu, R., Chen, Y.-F., 2023. Liquid cohesion induced particle agglomeration enhances clogging in rock fractures. Geophys. Res. Lett. 50 (5), e2022GL102097. https://doi.org/10.1029/2022GL102097.

Zhao, J., Shan, T., 2013. Coupled CFD–DEM simulation of fluid–particle interaction in geomechanics. Powder Technol. 239, 248–258. http://www.sciencedirect.com/science/article/pii/S0032591013001113.

Zhou, Y., Chen, L., Gong, Y., and Wang, S. (2021). "Pore-Scale Simulations of Particles Migration and Deposition in Porous Media Using LBM-DEM Coupling Method." *Processes*.

Zhou, Z., Kuang, S., Chu, K., Yu, A., 2010. Discrete particle simulation of particle-fluid flow: Model formulations and their applicability. J. Fluid Mech. 661, 482–510.

Zhou, W., Ma, Q., Ma, G., Cao, X., Cheng, Y., 2020. Microscopic investigation of internal erosion in binary mixtures via the coupled LBM-DEM method. Powder Technol. 376, 31–41. https://www.sciencedirect.com/science/article/pii/S0032591020307233.

Zhu, H.P., Zhou, Z.Y., Yang, R.Y., Yu, A.B., 2007. Discrete particle simulation of particulate systems: Theoretical developments. Chem. Eng. Sci. 62 (13), 3378–3396. https://www.sciencedirect.com/science/article/pii/S000925090700262X.

Zhu, H., Zhou, Z., Yang, R., Yu, A., 2008. Discrete particle simulation of particulate systems: A review of major applications and findings. Chem. Eng. Sci. - CHEM. ENG. SCI. 63, 5728–5770.